Non-linear Response of 2D Electron Systems at Low Temperatures to Electric and Magnetic fields

by

Natalia Romero Kalmanovitz

A dissertation submitted to the Graduate Faculty in Physics
in partial fulfillment of the requirements for the degree of
Doctor of Philosophy, The City University of New York
2009

This manuscript has been read and accepted for the
Graduate Faculty in Physics in satisfaction of the
dissertation requirement for the degree of Doctor of Philosophy.

6/4/09	Sergey A. Vitkalov
Date	Chair of Examining Committee
6/4/09	Steven Greenbaum
Date	Executive Officer

Carlos Meriles

Dimitri Garanin

Frederick Smith

David Schmeltzer
Supervisory Committee

THE CITY UNIVERSITY OF NEW YORK

Abstract

Non-linear Response of 2D Electron Systems at Low Temperatures to Electric and Magnetic fields

by

Natalia Romero Kalmanovitz

Adviser: Profesor Sergey A. Vitkalov

The nonlinear behavior of low-dimensional electron systems has attracted a great deal of attention for its fundamental interest as well as for potentially important applications in nanoelectronics. This work focuses on experimental results related to the nonlinear behavior of two dimensional electron systems. We first observed the non-linear zero-differential resistance state (ZDRS) that occurs for highly mobile two dimensional electron systems in response to a dc bias in the presence of a strong magnetic field applied perpendicular to the electron plane is suppressed. We found that it disappears gradually as the magnetic field is tilted away from the perpendicular at fixed filling factor. Good agreement is found with a model that considers the effect of the Zeeman splitting of Landau levels enhanced by the in-plane component of the magnetic field. Furthermore, we observed that when an electric field is applied to conductors, it heats electric charge carriers. It is demonstrated that an electric field applied to a conductor with a discrete electron spectrum produces a non-equilibrium electron distribution, which cannot be described by temperature. Such electron distribution changes significantly the conductivity of the electrons in a magnetic field, and forces them into a state with a zero differential resistance. Most importantly, the results demonstrate that in general, the effective overheating in the systems with discrete spectrum is significantly stronger than the one in systems with continuous and homogeneous distribution of the energy levels at the same input power. In the last part we observed non-linear behavior in a silicon MOSFET.

Measurements of the rectification of microwave radiation at the boundary between two-dimensional electron systems separated by a narrow gap on a silicon surface for different temperatures, electron densities and microwave power, were performed. A theory is proposed that attributes the rectification to the thermoelectric response due to strong local overheating by the microwave radiation at the boundary between two dissimilar 2D metals.

Acknowledgments

It is difficult to overstate my gratitude to my Ph.D. supervisor, Prof. Sergey Vitkalov. With his enthusiasm, his inspiration, his practical approach, and his great efforts to explain things clearly and simply, he helped me a lot with my work in the lab. I appreciate all his contributions of time, ideas, and funding to make my Ph.D. experience productive and stimulating. I would have been lost without him.

I would like to thank Prof. Myriam Sarachik. She patiently taught me how to write a paper and shared with me a lot of her expertise and research insight.

I would like to thank Dr. Ivan Larkin, without him most of the interpretations of the rectification data would not have been possible.

I would like to thank Jing-qiao Zhang for the numerous conversations about the lab work and physics and for his help with trouble shooting problems in the lab.

I would also like to thank the members of my thesis committee, Prof. Carlos Meriles, Prof. Dimitri Garanin, Prof. Frederick Smith , Prof. David Schmeltzer and Prof. Sergey Vitkalov for taking the time to read my thesis.

I thank my friends, Galit and Nirit, Meirav and Liat for their invaluable friendship.

I would like to thank my mother, Belinda, for her unconditional love, warmth and support. I would like to thank my step father Sergio for his support.

Finally, I would like to express special thanks to my husband Mark. He helped me to concentrate on completing this dissertation and gave me mental support during the course of this work. Without his help and encouragement this study would not have been completed.

This thesis is dedicated to the memory of my grandmother, Miriam.

Contents

List of Figures

1 Introduction

In this work experimental results of the non-linear properties of two dimensional electron systems are presented. Results for the non-linear zero-differential resistance state (ZDRS) that occurs for a GaAs quantum well [1] are shown. It is found that in response to a dc bias and in the presence of a strong magnetic field applied perpendicular to the electron plane, this ZDRS is suppressed and disappears gradually as the magnetic field is tilted away from the perpendicular at fixed filling factor ν. The experimental results were explained with the use of a theoretical model [2] that considers spectral diffusion of the electrons, as well as the effect of the Zeeman splitting of Landau levels enhanced by the in-plane component of the magnetic field.

Furthermore, the different results obtained when the electric field applied to a conductor is swept while maintaining a constant temperature, versus varying the temperature while keeping the electric field constant, are presented [3]. It is shown that the electric field applied produces a non-equilibrium electron distribution, very different to the effect obtained when the temperature is varied. This electron distribution changes significantly the conductivity of highly mobile two dimensional electron systems in the presence of a magnetic field, and it forces them into a state with a zero differential resistance. Moreover, the results demonstrate that in general, the effective overheating in systems with a discrete spectrum is much stronger than the one in systems with continuous and homogeneous distribution of the energy levels at the same input power.

Another non-linear effect is studied in a silicon MOSFET [4]. In this case we measured the effect of the rectification of microwave radiation ($0.7 - 20$ GHz) at the boundary between two two-dimensional electron systems separated by a narrow gap on a silicon surface for different temperatures, electron densities and microwave powers. It was

found that for frequencies above 4 GHz and different temperatures, the rectified voltage V_{dc} as a function of microwave power P can be scaled onto a single universal curve $V_{dc}^* = f^*(P^*)$. The scaled voltage is a linear function of power, $V_{dc}^* \propto P^*$ for small power and proportional to $(P)^{1/2}$ at higher power. A theory that attributes the rectification to the thermoelectric response due to strong local overheating by the microwave radiation at the boundary between these two dissimilar 2D metals was proposed.

In the following, we review the physical properties of a two dimensional electron gas (2DEG) at low temperatures and in the presence of electric and magnetic fields, as well as theoretical models which explain our experimental observations.

1.1 Modulation Doping and the 2D Electron Gas

The recent advances in the fabrication of tiny electronic devices has raised much interest in the quantum-mechanical aspects of their transport properties. These systems are patterned in a two-dimensional electron gas, which is formed in the planar interface between a semiconductor and an insulator, with a metallic layer under the insulator [5, 6]. Most popular is the two-dimensional electron gas formed in an AlGaAs/GaAs heterostructure, where it is located several tens of nanometers below the surface. Figure 1 shows a schematic view of the structure. The sheet carrier density, n, is typically of the order of $10^{12}\ cm^{-2}$, and the carrier mobility, μ, is about $10^5 - 10^7\ cm^2/Vs$. The Fermi wavelength of the electrons, $\lambda_F = 2\pi/k_F$, is typically tens of nm, and the mean-free-path, ℓ_e, of an electron at the Fermi level (the distance it travels before its initial momentum is destroyed) is of the order of a few microns.

The versatility of the fabrication techniques, such as molecular beam epitaxy (MBE) [7] and metal-organic vapor phase epitaxy (MOVPE) has made it possible to produce semiconductor 'quantum well' structures, where the composition changes on the scale of an atomic layer, with the band edge energies and carrier effective masses, conse-

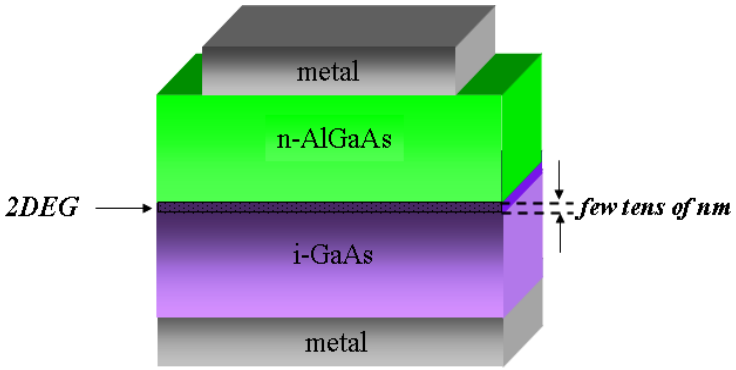

Figure 1: GaAs/AlGaAs heterostructure

.

quently, changing on the same length scale. The ability to physically separate dopant atoms from the layers where conduction occurs, so-called modulation doping, led to faster electronic devices, with improved transport characteristics. New physical effects were also found in low dimensional structures, including the quantum Hall effect and the fractional quantum Hall effect.

The conductivity [7] σ in a bulk semiconductor is given by

$$\sigma = ne\mu, \tag{1}$$

where n is the carrier density per unit volume and μ is the carrier mobility. The conductivity can be increased by increasing the doping density N_d. However, this will also increase the the number of ionized impurity scattering centers ($= N_d$), which will reduce the mobility. By contrast, the carrier density, n_s can be increased in a low dimensional system without significantly reducing the mobility through modulation doping. In this case, the dopant atoms are placed in a different layer to that in

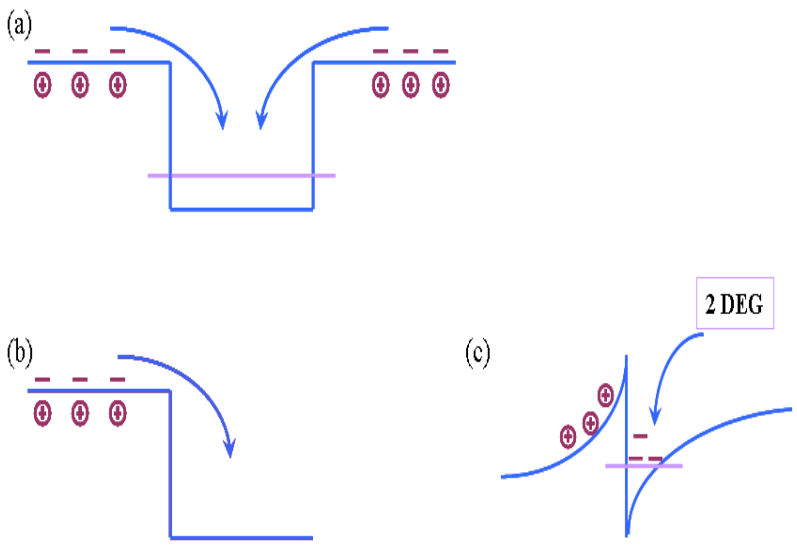

Figure 2: (a) When donor atoms are placed in the barrier layers adjacent to a quantum well, the excess donor electrons (-) can transferred into the quantum well, leaving the positively ionized impurity centers ($\oplus$) in the barrier. (b) A modulation doped heterojunction formed by doping a thin region of a wide-gap semiconductor close to the interface with a narrower gap material. (c) It is energetically favorable for the electrons to transfer into the narrower gap material. The electrons become confined due to the positively ionized impurity sites.

which the conduction is occurring. An example of modulation doping is depicted in Fig. 2(a) in a quantum well. A quantum well is often realized with a thin layer of a semiconductor medium, embedded between other semiconductor layers of wider band gap (for example, a GaAs quantum well embedded in AlGaAs, or InGaAs embedded in GaAs). The thickness of such a quantum well is typically $\approx 5-20$ nm. Both electrons and holes can be confined in these semiconductor quantum wells. In Fig. 2(a) donor atoms are placed in the barrier layers adjacent to a quantum well. The excess donor electrons are transferred into the quantum well, leaving the ionized impurity centers in the barrier.

By modulation doping one can also achieve two dimensional conduction at the heterojunction between two layers with different band gaps. For example, a thin layer of AlGaAs can be doped with an areal doping density N_s with the doping layer separated by an undoped spacer layer of width w from a neighboring GaAs region. (Fig. 2(b)). It is energetically favorable for the doping electrons to transfer into the narrower band gap GaAs layer, leaving behind positively charged donors. This space charge creates an electrostatic potential which makes the bands bend as shown in Fig. 2(c), where the thin conducting layer of confined electrons is called the two dimensional electron gas (2DEG). The carrier concentrations in a 2DEG range from $2 \times 10^{11}/cm^2$ to $2 \times 10^{12}/cm^2$, and can be depleted by applying a negative voltage to a metallic gate deposited on the surface.

The above structure is similar to that of a silicon MOSFET (metal-oxide-semiconductor field-effect transistor). In this case there is Si instead of GaAs, and AlGaAs is replaced by a thermally grown oxide layer (SiO_x).

1.2 Behavior of the resistance in the presence of electric and magnetic fields

Figure 3 shows [6] the longitudinal and transverse voltages as a function of magnetic field as measured by [8], for a modulation doped GaAs film at T= 2.1 K. At low magnetic fields, the longitudinal voltage is nearly constant while the Hall voltage increases linearly in agreement with the semi-classical Drude model. However, at high fields, the longitudinal resistance exhibits oscillatory behavior, while the Hall resistance exhibits plateaus corresponding to minima in the longitudinal resistance. These features are evident at low temperatures below 4 K.

In order to understand these features, we present the Drude model and continue with

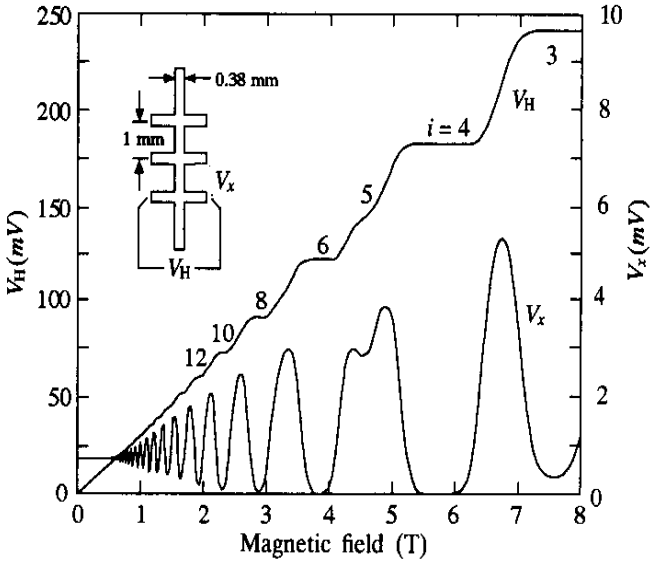

Figure 3: Measured longitudinal and transverse voltages for a modulation-doped GaAs film at $T = 1.2$ K ($I = 25.5\mu$A. E. Cage, R. F. Dziuba and B. F. Field (1985), IEEE Trans. Instrum. Meas. **IM-34**, 301.[6]

a discussion of the formation of Landau levels, a quantum mechanical effect which explains the behavior of the magnetoresistance at high magnetic fields.

1.2.1 The Drude model

The Drude model is a theory of metallic conduction [9] composed by Paul Drude. In this model the kinetic theory of gases is applied to a metal, considered as an electron gas, in order to deal with the electrical and thermal conductivity of the metal. Kinetic theory treats the molecules of a gas as identical solid spheres which move in straight lines until they collide with one another. The time taken by each collision is assumed to be negligible, and only the forces that act in each collision play a role. In the simplest gases there is only one kind of particle present. In a metal we must assume at least two kinds of particles because a metal is electrically neutral and the electrons have a negative charge.

The Drude model assumes a compensating positive charge attached to much heavier immobile particles. When atoms of a metallic element are brought together to form a metal, the valence electrons become detached and move freely through the metal, while the metallic ions remain intact and immobile. In an isolated atom the nucleus is surrounded by Z_α electrons of total charge $-eZ_\alpha$, where Z_α is the atomic number, e is the electronic charge. There are a few Z relatively weakly bound valence electrons. There are $Z_\alpha - Z$ electrons tightly bound to the nucleus, these are the core electrons. When these isolated atoms condense to form a metal, the core electrons remain tightly bound to the nucleus, while the valence electrons are free to move away from the core, these are the conduction electrons. The Drude model treats the dense metallic electron gas using the following basic assumptions:

1. Between collisions, each electron moves in a straight line in the absence of an externally applied electromagnetic field and electron-electron interactions and electron-ion

interactions are neglected.

2. Collisions in the Drude model are instantaneous events that abruptly alter the velocity of an electron. These collisions occur when electrons bounce off the impenetrable ion cores.

3. It is assumed that the electron experiences a collision (i.e. suffers an abrupt change in its velocity) with a probability per unit time $1/\tau_{tr}$, where τ_{tr} is called the momentum relaxation time, the collision time or the mean free time.

4. It is assumed that electrons achieve thermal equilibrium with their surroundings only through collisions. After each collision an electron is taken to emerge with a velocity that is not related to its velocity prior to the collision, but randomly directed.

The resistance in the presence of both electric and magnetic fields, according to the Drude model, is calculated in the following way: At steady state,[6] the rate at which electrons receive momentum from the external field is equal to the rate at which they lose momentum due to scattering forces,

$$\left[\frac{d\mathbf{p}}{dt}\right]_{scattering} = \left[\frac{d\mathbf{p}}{dt}\right]_{field}. \tag{2}$$

We may therefore write,

$$\frac{m\mathbf{v}}{\tau_{tr}} = e\left(\mathbf{E} + \mathbf{v} \times \mathbf{B}\right) \tag{3}$$

where τ_{tr} is the momentum relaxation time, m is the electron mass, $\mathbf{v}$ is the average electron velocity and $\mathbf{E}$ and $\mathbf{B}$ are the electric and magnetic fields. This leads to,

$$\begin{pmatrix} m/e\tau_{tr} & -B \\ B & m/e\tau_{tr} \end{pmatrix} \begin{pmatrix} v_x \\ v_y \end{pmatrix} = \begin{pmatrix} E_x \\ E_y \end{pmatrix} \tag{4}$$

The current $\mathbf{j}$ can be expressed as

$$\mathbf{j} = -ne\mathbf{v}, \tag{5}$$

where n is the electron density and e is the electron charge.

Combining Eq.(4) using Eq.(5),

$$\begin{pmatrix} m/e\tau_{tr} & -B \\ B & m/e\tau_{tr} \end{pmatrix} \begin{pmatrix} J_x/en \\ J_y/en \end{pmatrix} = \begin{pmatrix} E_x \\ E_y \end{pmatrix} \tag{6}$$

rearranging, we obtain

$$\begin{pmatrix} E_x \\ E_y \end{pmatrix} = \sigma^{-1} \begin{pmatrix} 1 & -\mu B \\ \mu B & 1 \end{pmatrix} \begin{pmatrix} J_x \\ J_y \end{pmatrix} \tag{7}$$

where the conductivity is given by $\sigma = en\mu$ and the mobility is given by $\mu = e\tau_{tr}/m$, so that $\sigma = ne^2\tau_{tr}/m$.

The resistivity tensor is defined by the relation

$$\begin{pmatrix} E_x \\ E_y \end{pmatrix} = \begin{pmatrix} \rho_{xx} & \rho_{xy} \\ \rho_{yx} & \rho_{yy} \end{pmatrix} \begin{pmatrix} J_x \\ J_y \end{pmatrix} \tag{8}$$

so that

$$\rho_{xx} = \sigma^{-1} \tag{9}$$

$$\rho_{yx} = -\rho_{xy} = \mu B/\sigma = B/en. \tag{10}$$

Thus, the Drude model predicts a constant longitudinal resistance and a Hall resistance that increases linearly with magnetic field.

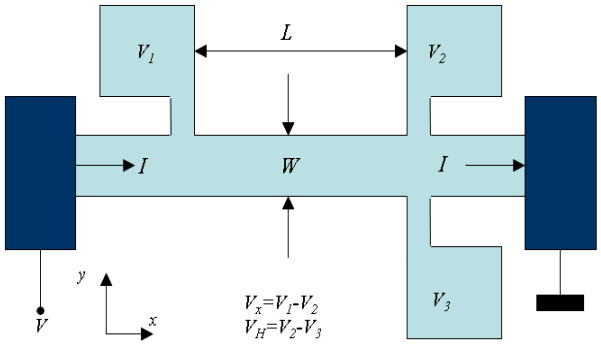

Figure 4: A schematic magnetoresistance and Hall effect measurement in a typical Hall bar. A current I is supplied from source to drain. V_H is supplied across the current, V_x along it.

1.2.2 High-field magnetoresistance

The Drude result for the resistivity tensor is given by [5]

$$\hat{\rho} = \begin{pmatrix} \sigma^{-1} & -B/en \\ B/en & \sigma^{-1} \end{pmatrix} \tag{11}$$

The resistivity tensor is measured in a Hall bar, shown in Fig. 4. A current flows in the x direction and the longitudinal voltage drop $V_x = V_1 - V_2$ and the transverse voltage drop $V_H = V_2 - V_3$, are measured. Therefore,

$$E_y = \rho_{xy} j_x = -\frac{B}{en} j_x, \quad V_H = -\frac{B}{en} I_x, \tag{12}$$

$$E_x = \rho_{xx} j_x = j_x/\sigma, \quad V_L = \frac{L}{W}\frac{I_x}{\sigma}, \tag{13}$$

for a sample with width W and length L, as in Fig. 4. B is perpendicular to the plane of the figure in the positive z direction, and assuming homogeneity, $I_x = j_x W$, $V_H = W E_y$, and $V_x = L E_x$.

The carrier density n and the mobility μ can be obtained from the measured low-field resistivities ρ_{xx} and ρ_{xy}, using Eq.(9) and Eq.(10),

$$n = (|e| d\rho_{yx}/dB)^{-1} = \frac{I/|e|}{dV_H/dB} \tag{14}$$

$$\mu = \frac{1}{|e| n \rho_{xx}} = \frac{I/|e|}{n V_x W/L} \tag{15}$$

The Shubnikov de Haas (SdH) oscillations

The oscillations in the longitudinal component of the resistivity ρ_{xx} in Fig. 3 are called Shubnikov de Haas (SdH) oscillations. These oscillations arise because at high magnetic fields, the step like density of states in a 2DEG

$$\nu_s(E, B) = \frac{m}{\pi \hbar^2} \Theta(E - E_s) \tag{16}$$

will break-up into a sequence of peaks spaced by $\hbar\omega_c$ (neglecting the Zeeman effect), where $\omega_c = eB/m$ is the cyclotron frequency.

$$\nu_s(E, B) \approx \frac{2eB}{h} \sum_{n=0}^{\infty} \delta(E - E_s - (n + \frac{1}{2})\hbar\omega_c). \tag{17}$$

In Fig. 5 the DOS is plotted as a function of energy. Ideally, the spikes should be delta functions, but in practice scattering processes spread them out in energy. This spread in energy is governed by τ_q, the single particle relaxation time due to scattering (mostly impurity scattering at low temperatures) at zero magnetic field, so that the Landau levels broaden into narrow bands with approximate width $\hbar/\tau_q$.

As the magnetic field B is changed, the energies of the Landau levels change. The

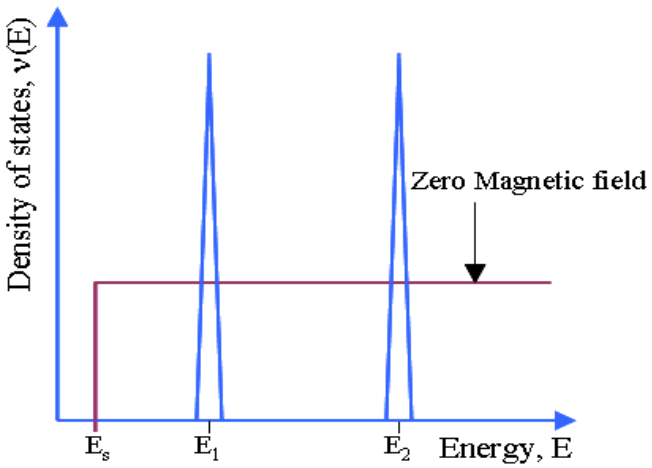

Figure 5: The density of states $\nu(\epsilon)$ as a function of energy ϵ for a 2DEG in a magnetic field. $\epsilon_n = \epsilon_s + (n + 1/2)\hbar\omega_c$.

resistivity ρ_{xx} goes through one cycle of oscillations as the Landau levels move and the Fermi energy goes through the center of one Landau level to the center of the next Landau level.

It can be seen from Eq.(17) that the electron density n can be calculated from the Shubnikov de-Haas oscillations. For a given electron density n, the number of occupied Landau levels can be calculated by dividing the electron density n by $2eB/h$. The ratio $n/(2eB/h)$ is the called the filling factor. As the magnetic field B is changed the number of occupied Landau levels changes. ρ_{xx} goes through a maximum every time this number is a half integer and the Fermi energy lies at the center of a Landau level. Therefore, the magnetic field values B_1 and B_2 corresponding to two successive peaks must be related by,

$$n/2eB_1/h - n/2eB_2/h = 1 \tag{18}$$

$$n = 2e/h\frac{1}{(1/B_1) - (1/B_2)} \tag{19}$$

1.2.3 The formation of Landau levels

In order to explain why the DOS develops peaks at high magnetic fields, we start from the Schrödinger equation including a vector potential representing the magnetic field and calculate its eigenfunctions and eigenvalues.

The motion of electrons in a conductor in the presence of a constant magnetic field is given by the effective mass equation, Eq.(20). The lattice potential, which is periodic on an atomic scale, does not appear explicitly in Eq.(20), its effect is incorporated through the effective mass m which we assume to be spatially constant:

$$\left(E_s + \frac{(i\hbar\nabla + e\mathbf{A})^2}{2m}\right)\Psi(x,y) = E\Psi(x,y), \tag{20}$$

where $E_s = E_c + \epsilon_1$, E_c is the conduction band energy, and ϵ_1 is the cut-off energy in

the z-direction, m is the effective mass, and $\mathbf{A}$ is the vector potential derived from $\mathbf{B}$, a constant magnetic field in the z-direction which may be represented by $\mathbf{A} = -\hat{x}By$, so that $A_x = -By$ and $A_y = 0$.

Therefore, we may write

$$\left(E_s + \frac{(p_x + eBy)^2}{2m} + \frac{p_y^2}{2m}\right)\Psi(x,y) = E\Psi(x,y), \tag{21}$$

where $p_x = -i\hbar\partial_x$, $p_y = -i\hbar\partial_y$. The solutions may be expressed as plane waves $\Psi(x,y) = 1/\sqrt{L}\exp[ikx]\,\chi(y)$. The function $\chi(y)$ satisfies the equation

$$\left(E_s + \frac{(\hbar k + eBy)^2}{2m} + \frac{p_y^2}{2m}\right)\chi(y) = E\chi(y). \tag{22}$$

This may be rewritten in the form

$$\left(E_s + \frac{1}{2}m\omega_c^2(y + y_k)^2 + \frac{p_y^2}{2m}\right)\chi(y) = E\chi(y) \tag{23}$$

where $y_k = \hbar k/eB$ and $w_c = eB/m$.

$$\chi_{n,k} = u_n(q + q_k) \tag{24}$$

where

$$u_n(q) = \exp[-q^2/2]H_n(q) \tag{25}$$

$H_n(q)$ are the Hermite polynomials, $q = \sqrt{mw_c/\hbar}y$ and $q_k = \sqrt{mw_c/\hbar}y_k$.

The energies are given by

$$E(n,k) = E_s + (n + \frac{1}{2})\hbar\omega_c, \quad n = 0, 1, 2..., \tag{26}$$

where the Landau levels (or magnetic subbands) are indexed by n.

1.3 The Boltzmann equation

The Boltzmann equation provides a more complete and consistent description of the electron transport for overheated and spatially non-uniform electron systems. The motion of electrons in metals and semiconductors is affected by temperature gradients and external fields, as well as by the scattering of these electrons with lattice waves and impurities [10]. In this treatment we consider a case where an electron is accelerated by a field, therefore gaining extra energy and momentum, and then loses this extra energy and momentum in scattering processes. The Boltzmann equation gives a general solution to this problem.

We look at the quantity $f_{\mathbf{k}}(\mathbf{r})$, where $f_{\mathbf{k}}(\mathbf{r})$ gives us the local concentration of carriers in the state $\mathbf{k}$, in the neighborhood of a point $\mathbf{r}$ in space.

This analysis accounts for three types of effects which cause changes in $f_{\mathbf{k}}(\mathbf{r})$ with time:

1. Carriers moving in and out of the region $\mathbf{r}$. If we denote the velocity of a carrier in a state $\mathbf{k}$ by $\mathbf{v_k}$, then in a time interval t, the carriers in this state move a distance $t \cdot \mathbf{v_k}$. Assuming the invariance of volume occupied in phase space (Liouville's theorem), then the number of carriers in the neighborhood of r at time t is equal to the number of carriers in the neighborhood of $\mathbf{r} - t\mathbf{v_k}$ at time zero,

$$f_{\mathbf{k}}(\mathbf{r}, t) = f_{\mathbf{k}}(\mathbf{r} - t\mathbf{v_k}, 0). \tag{27}$$

The rate of change of $f_{\mathbf{k}}(\mathbf{r})$ due to diffusion is

$$\frac{\partial f_{\mathbf{k}}}{\partial t}_{diff.} = -\mathbf{v_k} \nabla f_{\mathbf{k}}. \tag{28}$$

2. External fields change the **k**-vector of each carrier, at a rate

$$\dot{\mathbf{k}} = -\frac{e}{\hbar}(\mathbf{E} + \frac{1}{c}\mathbf{v_k} \times \mathbf{H}) \tag{29}$$

this may viewed as the velocity of the carriers in **k**-space, so that according to Liouville's theorem,

$$f_{\mathbf{k}}(\mathbf{r}, t) = f_{\mathbf{k}-\dot{\mathbf{k}}t}(\mathbf{r}, 0) \tag{30}$$

so that due to the fields the distribution changes at a rate:

$$\frac{\partial f_{\mathbf{k}}}{\partial t}_{field} = -\dot{\mathbf{k}}\frac{\partial f_{\mathbf{k}}}{\partial \mathbf{k}} = -\frac{e}{\hbar}(\mathbf{E} + \frac{1}{c}\mathbf{v_k} \times \mathbf{H})\frac{\partial f_{\mathbf{k}}}{\partial \mathbf{k}} \tag{31}$$

3. Electron scattering will give rise to a rate of change of $f_{\mathbf{k}}$. In order to calculate this term we often make the phenomenological assumption

$$\frac{\partial f_{\mathbf{k}}}{\partial t}\Big]_{scatt} = -\frac{f_{\mathbf{k}} - f^0_{\mathbf{k}}}{\tau} \tag{32}$$

where f^0_k is the Fermi distribution function. We have introduced a relaxation time τ. This approximation is called *the relaxation time approximation*.

The Boltzmann equation says that at any point, and for any value of **k**, the net rate of change of $f_{\mathbf{k}}(\mathbf{r})$ is given by

$$\frac{\partial f_{\mathbf{k}}}{\partial t} = \frac{\partial f_{\mathbf{k}}}{\partial t}\Big]_{scatt.} + \frac{\partial f_{\mathbf{k}}}{\partial t}\Big]_{field} + \frac{\partial f_{\mathbf{k}}}{\partial t}\Big]_{diff.} \tag{33}$$

The term in the left hand side of the equation, $\partial f_{\mathbf{k}}/\partial t$ represents the net rate of change of the distribution function, and will be zero at steady state. The equilibrium state $f^0_{\mathbf{k}}$ holds when the net rate of change of the distribution function, fields and temperature gradients are zero.

Inserting Eq.(32) into Eq.(33) yields,

$$\frac{\partial f_{\mathbf{k}}}{\partial t} + \dot{\mathbf{k}} \cdot \frac{\partial f_{\mathbf{k}}}{\partial \mathbf{k}} + \mathbf{v}_{\mathbf{k}} \cdot \nabla f_{\mathbf{k}} = -\frac{f_{\mathbf{k}} - f^0_{\mathbf{k}}}{\tau} \tag{34}$$

1.3.1 Calculation of the electrical conductivity

The electron current density is given by [10]

$$\mathbf{J} = 2 \int e\mathbf{v} f d\mathbf{k} = \sigma \cdot \mathbf{E}. \tag{35}$$

In a stationary state and in the presence of an electric field we get from Eq.(29) and Eq.(34) (note that the subscript k has been omitted in the following treatment for simplicity)

$$\frac{f - f^0}{\tau} = -\frac{e}{\hbar}\mathbf{E} \cdot \frac{\partial f}{\partial \mathbf{k}} = -\frac{e}{\hbar}\mathbf{E} \cdot \frac{\partial f}{\partial \epsilon}\frac{\partial \epsilon}{\partial \mathbf{k}} \tag{36}$$

where f is the non-equilibrium distribution function and f^0 is the equilibrium distribution function (the Fermi distribution function). With the use of the relation $\mathbf{v} = (1/\hbar)\partial\epsilon/\partial\mathbf{k}$, we obtain

$$f = -e\tau\frac{\partial f}{\partial \epsilon}\mathbf{E} \cdot \mathbf{v} + f^0 \tag{37}$$

inserting this result into Eq.(35) yields

$$\mathbf{J} = \sigma \cdot \mathbf{E} = -2e^2 \int \tau\frac{\partial f}{\partial \epsilon}\mathbf{v}(\mathbf{E} \cdot \mathbf{v})\nu d\mathbf{k} + 2e \int f^0 \mathbf{v} d\mathbf{k} \tag{38}$$

the second term on the right hand side of Eq.(38) is zero. The integral Eq.(35) in ϵ-space is

$$\mathbf{J} = -\int \frac{e^2\tau m}{\pi\hbar^2}\frac{\partial f}{\partial \epsilon}\mathbf{v}(\mathbf{E} \cdot \mathbf{v})d\epsilon \tag{39}$$

For an electric field directed along the x-direction $\mathbf{E} = E_x$, $< v_x^2 >= v^2/2$ (in 2D),

therefore

$$\sigma_{xx} = -\int (\frac{e^2 \tau m v^2}{2\pi\hbar^2}) \frac{\partial f}{\partial \epsilon} d\epsilon. \tag{40}$$

We note that when $\epsilon = \epsilon_F$, $v = v_F$ and $\nu_0 = m/\pi\hbar^2$. We also have the relations $n = \epsilon_F \nu_0$ and $v_F^2 = 2\epsilon_F/m$, so that the term in the parenthesis is just the Drude conductivity, $\sigma_D = ne^2\tau/m$. We therefore denote the term in the parenthesis as $\sigma(\epsilon)$, namely, the conductivity as a function of energy. Thus, we may rewrite Eq.(40) as

$$\sigma_{xx} = \int \sigma(\epsilon)(-\frac{\partial f}{\partial \epsilon}) d\epsilon. \tag{41}$$

1.4 Non-linear resistance induced by a dc electric field

In highly mobile electron systems strong oscillations of the longitudinal resistance induced by microwave radiation have been observed [11, 12] at magnetic fields satisfying the condition $w = nw_c$, where w is the microwave frequency and w_c is the cyclotron frequency ($n = 1, 2, ...$). At high levels of microwave excitation the minima of the oscillations can reach a value close to zero [13, 14, 15, 16]. This so-called zero resistance state (ZRS) has stimulated extensive theoretical attention [2, 17, 18, 19, 20, 21, 22]. Interesting nonlinear phenomena have also been found in response to a dc electric field [23, 24, 25, 26]. Periodic oscillations of the longitudinal resistance, as a function of the inverse magnetic field, have been observed at relatively high dc bias satisfying the condition $n\hbar w_c = 2R_c E_H$; here R_c is the cyclotron radius of electrons at the Fermi level and E_H is the Hall electric field induced by the dc bias in the magnetic field. This effect has been attributed to horizontal Landau-Zener tunneling between Landau levels, tilted by the Hall electric field E_H [23].

Another notable nonlinear effect is a strong reduction of the longitudinal resistance by

dc electric fields [24, 25, 26]. This effect has been attributed [25] to spectral diffusion of electrons in a dc electric field [22]. This effect also accounts for a nonlinear electron state with zero differential resistance (ZDRS) which has been recently observed [27, 28]. The ZDRS exhibits strong dependences on both temperature and magnetic field [27] through the strong dependence of the electron spectral diffusion on these parameters [22, 25, 29]. In the following, a theoretical treatment of the effect of a dc electric field on the resistance in a magnetic field, is presented.

1.5 Theory of the dc electric field induced non-linear resistance

In this treatment, we look at the effect of a dc electric field on the electron distribution function with the use of the Boltzmann equation. The effect that the magnetic field has on the electron distribution function is introduced through the change in the density of states due to Landau quantization. We start by analyzing the relationship between the conductivity and resistivity tensors, and it will be shown that at high magnetic fields the longitudinal conductivity and the longitudinal resistivity are proportional to one another.

The conductivity and resistivity tensors are related by

$$\sigma_{xx} = \frac{\rho_{xx}}{\rho_{xx}^2 + \rho_{xy}^2}, \quad \sigma_{xy} = \frac{\rho_{xy}}{\rho_{xx}^2 + \rho_{xy}^2} \tag{42}$$

in the high magnetic field limit, $\omega_c \tau_{tr} >> 1$ and $\rho_{xx} << \rho_{xy}$, where τ_{tr} is the transport scattering time, or relaxation time, this is scattering with impurities, lattice vibrations (phonons), or other electrons which lead to a change in momentum. We may therefore neglect the terms ρ_{xx} in both denominators and obtain for the longitudinal conductivity

$$\sigma_{xx} = \rho_{xx}/\rho_{xy}^2. \tag{43}$$

Thus, according to Eq.(43), the classical magnetoresistance is given by $\sigma_D = r_0/\rho_{xy}^2$, where r_0 is the resistance at zero field (this is because in the classical regime the longitudinal resistance is constant). We get

$$\sigma_{xx}/\sigma_D = \rho_{xx}/r_0, \tag{44}$$

we therefore obtain that the longitudinal conductivity and the longitudinal resistivity are *proportional* to one another.

Consequently, the longitudinal resistance ρ_{xx} can be obtained by using a simplified expression for the longitudinal conductivity in strong magnetic fields ($\omega_c\tau_{tr} \gg 1$): [22] (see Eq.(41))

$$\sigma_{xx} = \int \sigma_{dc}(\epsilon)(-df/d\epsilon)d\epsilon, \tag{45}$$

$f(\epsilon)$ is the electron distribution function, and $\sigma_{dc}(\epsilon)$ determines the contribution of electrons with energy ϵ to the transport. σ_{xx} determines the longitudinal current that flows in response to a dc electric field.

In order to calculate $\sigma_{dc}(\epsilon)$, we start from the Drude results for the resistivities $\rho_{xx} = m/ne^2\tau_{tr,B}$ and $\rho_{xy} = B/en$. We then obtain,

$$\sigma_{dc}(\epsilon) = \frac{\rho_{xx}}{\rho_{xx}^2 + \rho_{xy}^2} = \frac{e^2\nu(\epsilon)v_F^2}{2}\frac{\tau_{tr,B}^{-1}(\epsilon)}{\omega_c^2 + \tau_{tr,B}^{-2}(\epsilon)}, \tag{46}$$

τ_{tr} was replaced with the scattering time in a quantizing magnetic field $\tau_{tr,B}(\epsilon) = \tau_{tr}\nu_0/\nu_(\epsilon)$, and $\nu_0 = m/2\pi$ is the DOS per spin at zero magnetic field (here we use $\hbar = 1$ and $c = 1$), and $\omega_c = eB/m$.

For strong magnetic fields $\omega_c\tau_{tr} >> 1$,

$$\sigma_{dc}(\epsilon) = \sigma_{dc}^{D}\tilde{\nu}^2(\epsilon) \tag{47}$$

$\sigma_{dc}^{D} = e^2\nu_0 v_F^2/2\omega_c^2\tau_{tr}$ is the Drude conductivity per spin in strong B and $\tilde{\nu}(\epsilon)$ is the dimensionless DOS, $\tilde{\nu}(\epsilon) = \nu(\epsilon)/\nu_0$.

We can calculate the non-equilibrium distribution function $f(\epsilon)$ in Eq.(45) by solving the stationary kinetic Boltzmann equation (see Eq.(29) and Eq.(34)) [22]

$$\frac{\partial f}{\partial t} + e\mathbf{E}_{dc}\cdot\frac{\partial f}{\partial \mathbf{p}} = -\frac{f - f^0(\epsilon)}{\tau_{in}} \tag{48}$$

The right hand side of Eq.(48) denotes the term of inelastic scattering. $f^0(\epsilon)$ is the Fermi distribution function and E_{dc} is the bias-induced electric field, τ_{in} is the inelastic scattering time and at low temperatures it is mainly due to e-e scattering or e-phonon scattering.

Impurity scattering in a quantizing magnetic field leads to spatial diffusion with a diffusion coefficient $D_B(\epsilon) = v_F^2\nu(\epsilon)/2w_c^2\tau_{tr}\nu_0 = v_F^2/2w_c^2\tau_{tr,B}(\epsilon)$ (this comes from the Einstein relation $\sigma_{dc}(\epsilon) = e^2\nu(\epsilon)D_B(\epsilon)$ together with Eq.(47)), so that $D_B(\epsilon) \propto \nu(\epsilon)$. In a dc field directed along the x-axis the total energy $\epsilon + eE_{dc}x$ is conserved, so that the spatial diffusion is translated into diffusion in energy space with a diffusion coefficient $D_\epsilon(\epsilon) = e(E_{dc})^2 D_B(\epsilon) \propto \nu(\epsilon)$. By making the expansion

$$f(\epsilon) = f^0(\epsilon) - (e\mathbf{E}_{dc}\cdot\mathbf{v}\tau_{tr})\frac{\partial f}{\partial \epsilon} + \frac{1}{2}(e\mathbf{E}_{dc}\cdot\mathbf{v}\tau_{tr})^2\frac{\partial^2 f}{\partial \epsilon^2} + ... \tag{49}$$

together with Eq.(48), and after some algebraic manipulations, we obtain the equation for the electron diffusion in energy space (spectral diffusion) at steady state

$$-\frac{\partial f(\epsilon)}{\partial t} + E_{dc}^2 \frac{\sigma_{dc}^D}{\nu_0 \tilde{\nu}(\epsilon)} \partial_\epsilon \left[\tilde{\nu}^2(\epsilon) \partial_\epsilon f(\epsilon) \right] = \frac{f(\epsilon) - f^0(\epsilon)}{\tau_{in}}, \tag{50}$$

Eq.(50) can be explained as follows: spectral diffusion is a result of elastic scattering between electrons and impurities in the presence of a bias-induced electric field E_{dc}; it is limited by inelastic processes, which force the distribution function back to thermal equilibrium.

Spectral diffusion generates an electron spectral flow J_ϵ from low energy regions (occupied levels) to high energies (empty levels). The spectral flow is proportional to $D_\epsilon(\epsilon)$ and to the gradient of the distribution function $df/d\epsilon$: $J_\epsilon = D_\epsilon \cdot df/d\epsilon$. In a stationary state the spectral electron flow J_ϵ is constant. Because $D_\epsilon(\epsilon) = e(E_{dc})^2 D_B(\epsilon) \propto \nu(\epsilon)$, the spectral (and spacial) diffusion is most effective in the center of the Landau levels, where the density of states is high, gradually decreases away from the center and is suppressed considerably between Landau levels, where the density of states is low. As a result, the gradient of the distribution function $df(\epsilon)/d\epsilon$ is strong in the regions of weak spectral diffusion (between Landau levels) and is small in the regions with strong spectral diffusion (centers of the Landau levels).

2 Experimental Techniques

In this section the experimental techniques and devices used in our experiments are presented in detail.

2.1 The Lock-in Amplifier

We used a Standford Research System model SR-830 Lock-In amplifier in our measurements. Lock-in amplifiers are used to detect and measure AC signals as small as a few nanovolts. Accurate measurements may be made even when the signal is obscured by noise sources many thousands of times larger. Lock-in amplifiers use a technique known as phase-sensitive detection to single out the component of the signal at a specific reference frequency and phase. Noise signals at frequencies other than the reference frequency are rejected and do not affect the measurement.

According to Fourier's theorem, any input signal can be represented as the sum of many sine waves of differing amplitudes, frequencies and phases. The SR830 multiplies the signal by a pure sine wave at the reference frequency. All components of the input signal are multiplied by the reference simultaneously. Due to the orthogonality of sine waves of different frequencies, the product of this multiplication yields a DC output signal proportional to the component of the signal whose frequency is exactly locked to the reference frequency. The low pass filter which follows the multiplier provides the averaging which removes the products of the reference with components at all other frequencies.

Typically a sample is excited at a fixed frequency and the lock-in detects the response from the sample at the reference frequency. For example, the reference signal may be a square wave at frequency ω_r. If the sine output from a function generator is used to excite the sample, the signal is $V_{sig}sin(\omega_r t + \theta_{sig})$ where V_{sig} is the signal amplitude.

The SR830 generates its own sine wave. The lock-in reference is $V_L sin(\omega_L t + \theta_{ref})$. The SR830 amplifies the signal and then multiplies it by the lock-in reference using a phase-sensitive detector or multiplier. The output of the PSD is simply the product of two sine waves:

$V_{psd} = V_{sig} V_L sin(\omega_r t + \theta_{sig}) sin(w_L t + \theta_{ref}) = 1/2 V_{sig} V_L cos([\omega_r - \omega_L]t + \theta_{sig} - \theta_{ref}) - 1/2 V_{sig} V_L cos([\omega_r + \omega_L]t + \theta_{sig} + \theta_{ref})$

The PSD output is then passed through a low pass filter, the AC signals are removed. If $\omega_r = \omega_L$, the difference frequency component will be a DC signal. In this case, the filtered PSD output will be $V_{psd} = 1/2 V_{sig} V_L cos(\theta_{sig} - \theta_{ref})$. This is a signal proportional to the signal amplitude.

Therefore, we need to make the lock-in reference the same as the signal frequency, i.e. $\omega_r = \omega_L$. Not only do the frequencies have to be the same, the phase between the signals can not change with time, otherwise $cos(\theta_{sig} - \theta_{ref})$ will change and V_{psd} will not be a DC signal. In other words, the lock-in reference needs to be phase-locked to the signal reference.

2.2 The Low Temperature Refrigerator

He^3 System

In our experiments we often performed measurements for temperatures below 1 K. The simplest way for reaching temperatures below 1K [30] is by using a ^3He evaporation cryostat. Whereas by pumping on a liquid bath of ^4He a temperature of approximately 1 K can normally be obtained, the lower limit with ^3He is slightly below 0.3 K.

The rule of cooling is directly described by thermal dynamics. At low temperatures the molar volume of a liquid, for example ^3He, may be neglected in comparison with the molar volume of the vapor, which approximately obeys the ideal gas law. The Clausius-Clayperon equation then becomes

$$dP_{v3}/dT = L_3(T)\, P_{v3}/RT^2 \tag{51}$$

where $L_3(T)$ is the latent heat of evaporation per mole and R is the gas constant. Furthermore, at low temperatures $L_3(T) \cong L_3(0)$ =constant. Eq.(51) may then be integrated to yield

$$P_{v3} \propto \exp\left[-L_3(0)/RT\right] \tag{52}$$

The vapor pressure thus decreases exponentially as a function of T. As the evaporation pressure is reduced by pumping, the bath temperature decreases.

This type of relation is valid for all substances. When a liquid bath is pumped, the cooling produced per unit mass crossing the liquid-vapor phase boundary is approximately constant, which is $L(0)$ per mole. However, the mass flow across the boundary and through the pump per unit time is proportional to the vapor pressure, hence the cooling power decreases exponentially with T. When equilibrium is reached, the vapor pressure becomes so low that the external heat leak will compensate the produced cooling. Thus, the practical low temperature limit of cooling by evaporation is reached. Two advantages of ^3He material result in the lower temperature limit of refrigerators. Firstly, because of its smaller mass, the ^3He atom has larger zero point motion than ^4He. Consequently P_{v3}, the vapor pressure of ^3He, is at all temperatures higher than the vapor pressure of ^4He. The ratio P_{v3}/P_{v4} is 74 at 1 K, 610 at 0.7 K, and 9800 at 0.5 K. Secondly, the critical temperature of the ^3He super fluid is much lower than the temperature of ^4He. That means there is no ^3He liquid film at rather low temperatures (lower than 1 mK). As a result, there is no extra heat leak due to heat transfer along, or evaporation of, the film. A ^3He system may thus be pumped via a wide tube at the low temperature end, without the need for a narrow constriction to

suppress the film flow. For ^3He, the practical low temperature limit is usually 0.3 K or slightly below.

The following table gives us the main properties of ^3He:

The main properties of ^3He

boiling point	3.19K	$T_{critical}$	3.32K
molar volume	37 cm^3 (1K)	latent heat	21J/mol (0.3K)

2.3 The Super Conducting Magnet

In our cryostat, a custom designed 90 kilogausss magnet at 4.2 K is installed. The super conducting magnet was built using a twisted multi filamentary NbTi wire in a copper matrix. The copper matrix in the wire acts as a form of quench protection along with the diodes.

Superconducting Magnets and Cryogenic Systems

Superconducting magnets must operate below both the critical temperature and the critical field of the material from which they are constructed.

For a superconducting magnet manufactured using NbTi, operation in the superconducting state is only possible below the surface indicated in Fig. 6. As long as a superconducting magnet operates beneath the surface shown in Fig. 6, the superconducting state is maintained and the magnet operates properly. However, if one tries to operate the magnet above this surface, a quench will occur, that is, there will be a transition back to the normal (resistive) state. This resistive region will quickly heat up due to a high current through it and the resistive region (called a *normal zone*) will propagate until a) all of the energy stored in the magnet is dissipated or b) the entire magnet becomes resistive or c) sufficient cooling is provided to stop propagation. Usually either (a) or (b) occurs resulting in a complete quench of the magnet.

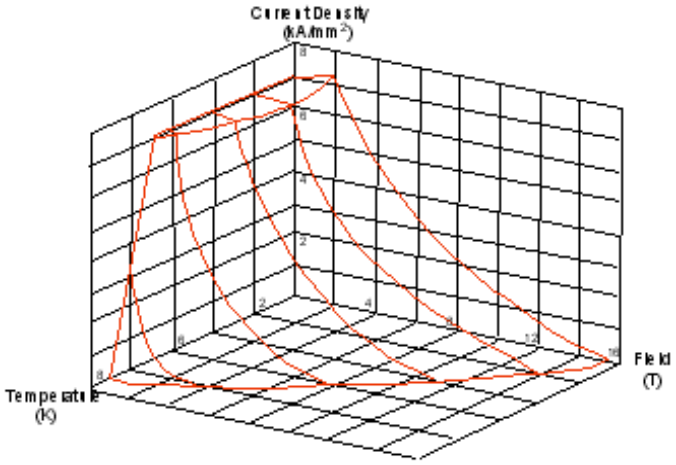

Figure 6: Niobium-Titanium superconducting properties

Stored Energy

The amount of energy stored in a magnet is a direct function of its geometry and operating conditions. The amount of energy is

$$W = \frac{1}{2} L I^2 \tag{53}$$

where L is the magnet's inductance, I is the operating current, and W is the energy. Most laboratory magnets have maximum stored energies on the order of $1000 - 100000$ Joules. Larger magnets are capable of storing several million Joules.

Superconducting magnets must always be designed with the amount of stored energy capability in mind. This is because when a quench occurs, this energy is converted to heat (usually in the windings) over a period of about a few seconds at most. This rapid conversion can induce not only high temperatures in the windings, but also high

voltages if they are not properly controlled. External devices are frequently used to help distribute the heat generated in a quench over the entire magnet windings. A rapid normal zone propagation is usually the key to distributing the heat generated and thus preventing it from becoming localized and damaging the superconductor.

Forces within magnets

When a superconducting magnet is charged, there are many forces which begin acting upon it. The force on a current-carrying wire in a magnetic field is given by $\mathbf{F} = \mathbf{I} \times \mathbf{B}$, where F is the force, and B is the field. Since there is usually a considerable current in a superconducting magnet's windings and it is generating high magnetic fields, it follows that the forces between the windings can become extreme. These forces try to force the wires within a superconducting magnet to move. This movement must be completely restrained because even the smallest wire movement will generate heat due to friction and can quench the magnet. In order to restrain the wire movements most superconducting magnets are potted using epoxy, ceramic, or some other material.

Persistent Mode

Our magnet is equipped with a Persistent Switch, which is a piece of superconducting wire with heater shorts its input power terminals. Superconducting magnets have one capability over resistive magnets. Once a current has been placed inside the magnets, virtually no power is need to maintain that current. When the magnet is being charged, the persistent switch heater is turned on so the short across the magnet terminals is driven above its critical temperature and effectively becomes a resistor across the magnet terminals. When the appropriate operating current in the magnetic is reached, the heater can be shut off and the persistent switch could be allowed to cool until it becomes superconducting. At this point the power source to the magnet is no longer needed.

Persistent mode operation has many advantages, mainly that the heat load on the

cryostat can be reduced by turning off the power supply, and that the stability of the magnetic field is very good in the persistent mode.

2.4 Microwave Transmission

In part of our experiments we used microwave signals in order do measure the effect of AC electric fields on our sample. Microwaves are electromagnetic waves with wavelengths ranging from 1 mm to 30 cm and frequencies between 0.3 GHz and 300 GHz. We used in our experiments a coaxial line and a waveguide in order to transmit the microwave field.

Coaxial Lines

In the coaxial structure, the outer conductor shields the inner conductor and prevents disturbances from the outside. In our experimental setup, 0.15" coaxial lines are used, suitable to transmit microwave frequencies of up to 40 Ghz.

Waveguides

The rectangular waveguide is a hollow conducting tube of rectangular cross section in which electromagnetic waves propagate.

The modes of propagation of the rectangular waveguide are the TE (Transverse Electric) and the TM (Transverse Magnetic) modes. The most commonly used mode is the TE_{10} mode since it has the lowest attenuation of all modes. Figure 7 shows the field distribution of the mode TE_{10}.

2.5 The Electronic System

The measurement system is composed of several parts: AC Lock-In amplifiers, driving current circuits and a four-point probe measurement circuit. A current is applied through the source and drain of samples and the potential difference of the sample

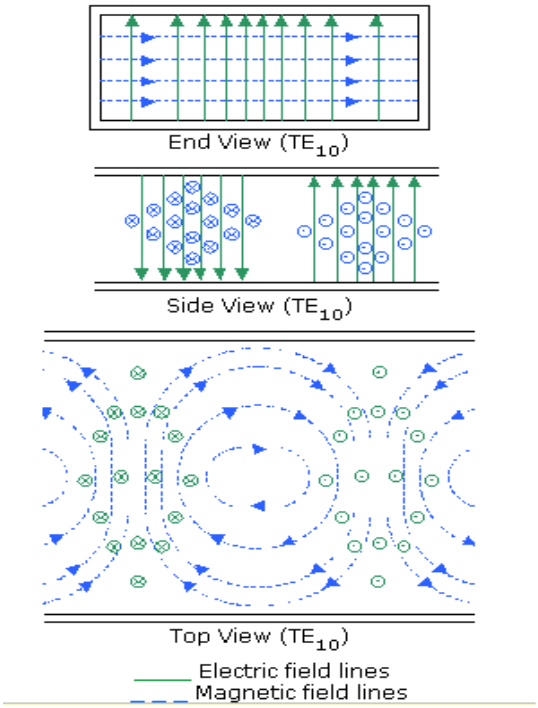

Figure 7: The TE_{10} mode in a rectangular waveguide

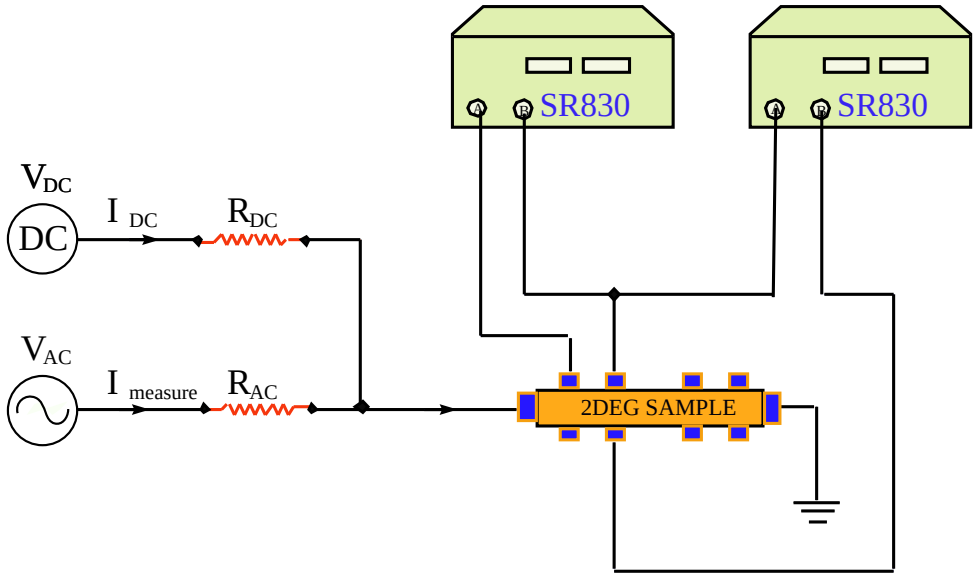

Figure 8: The electrical connections in our experiments.

area is measured.

The measurement system used in our experiments is depicted in Fig. 8 [30]. A Standford Research Systerm model SR-830 Lock-In amplifier provides the weak and low frequency AC current that flows through the source and drain in the sample by placing a big resistor in series with the sample. In order to regulate the driving current accurately, the resistor must be much bigger than the resistance variation in the experiments. Usually, we selected 10 MΩ or 400 MΩ resistors. The strength of the driving current is carefully selected by keeping in mind that the driving current should not heat-up the sample significantly while providing the highest signal-to-noise ratio attainable. In our measurements we selected a driving current frequency that minimizes the outphase signal created by the capacitor in the transmission line.

The CS-4 Cryomagnetics power supply provides the necessary current for super conducting magnets, which is a four-quadrant power supply and able to generate a smooth

field sweep. An Anritsu 68369A/NV microwave generator provides the AC signal from 100 Mhz to 40 Ghz with a 100 kHz resolution.

A SRS SIM 921 AC bridge was used to measure the temperature in the ^3He pot and a SRS SIM 9600 PID controller was used to control the temperature of the ^3He pot. This system provides a 1% precision in temperature measurements and control. In order to monitor the temperature of the sorbtion pump we used a BTI potentiometric conductance bridge/controller model 1000. The temperature of other parts of the system was monitored by Agilent 34401A multimeters.

2.5.1 Data Acquisition Software

The data acquisition software was written in Labview. All instruments were accessed through the GPIB interface. The block diagram of the software is depicted in Fig. 9 [30].

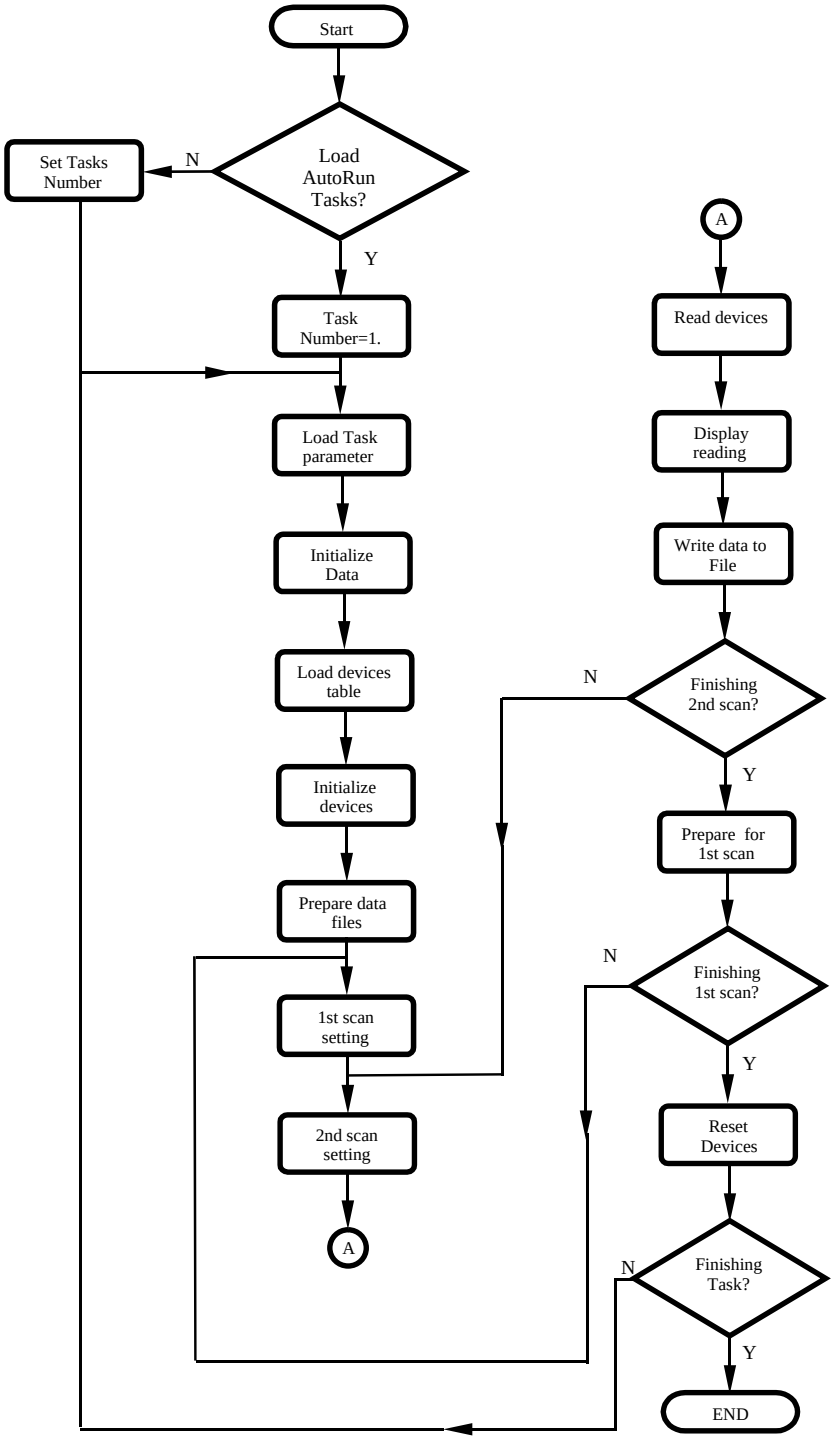

Figure 9: Flow chart of the data acquisition software

3 Effect of a parallel magnetic field on the Zero Differential Resistance State

3.1 Introduction

In section 1.4 we reviewed the non-linear zero-differential resistance state (ZDRS) which occurs for highly mobile two-dimensional electron systems in response to a dc bias and in the presence of a strong magnetic field applied perpendicular to the electron plane. Below [1] we demonstrate that the ZDRS is suppressed and disappears gradually as the magnetic field is tilted away from the perpendicular,while keeping the perpendicular component of the magnetic field, $B_\perp$, fixed (i.e. at a fixed filling factor ν).

In this work we studied the effect of an in-plane magnetic field on the ZDRS and the nonlinearity of the 2D electron system induced by a dc bias. We used a model that takes into account the effect of Zeeman splitting on the Landau levels. Zeeman splitting depends on the *total* magnetic field through $\Delta_Z = g\mu_B B$. In order to keep the perpendicular component of the magnetic field constant, we increased the total magnetic field. Therefore, the effect of Zeeman splitting was enhanced with the magnetic field tilt. This effect was incorporated into our theoretical model through the formulation of the density of states. As discussed in the introduction section, the density of states is modulated due to the applied magnetic field. In our model, we used a gaussian approximation for the density of states. We inserted our result for the DOS into the spectral diffusion equation in order to find the non-equilibrium electron distribution function. This allowed us to find the resistivity as a function of the applied electric dc field. We then found the resistance by simple integration. Our results of the resistance as a function of the dc field were calculated for different magnetic field

angles. We found good agreement between theory and experiment.

3.2 Experimental Setup

The sample used in this experiment was cleaved from a wafer of a high-mobility GaAs quantum well grown by molecular beam epitaxy on a semi-insulating (001) GaAs substrate. The quantum well was 13 nm wide, the electron density n= 9.2×10^{15} m^{-2}, and the mobility μ=85 m^2/Vs at T= 1.7 K. Measurements were carried out at T= 1.7 K in magnetic fields up to 9 T . We used 50μm-wide Hall bars with a distance of 250 μm between potential contacts. The differential longitudinal resistance was measured at a frequency of 77 Hz in the linear regime. Direct electric current (dc bias) was applied simultaneously with an ac excitation through the same current leads as shown in the inset of Fig. 10.

3.3 Experimental Results

Figure 10 shows quantum oscillations of the resistance at T= 1.7 K as a function of a magnetic field applied perpendicular to the electron plane (ϕ =90^o). The arrow denotes a Shubnikov de Haas maximum at $B_\perp = 0.772$ T.

In Fig. 11 the resistance R_{xx} is plotted as a function of the perpendicular component $B_\perp$ for a magnetic field applied at different angles with respect to the plane. While all curves display a maximum at $B_\perp = 0.772$ T, as expected, the magnitude of the resistance peaks at $B_\perp = 0.772$ T decreases as the angle ϕ decreases from 90^o and the total magnetic field increases.

For the measurements reported below, we rotated the sample and simultaneously varied the magnitude of the total magnetic field in order to fix the perpendicular magnetic field component at 0.772 T while changing the in-plane magnetic field. The

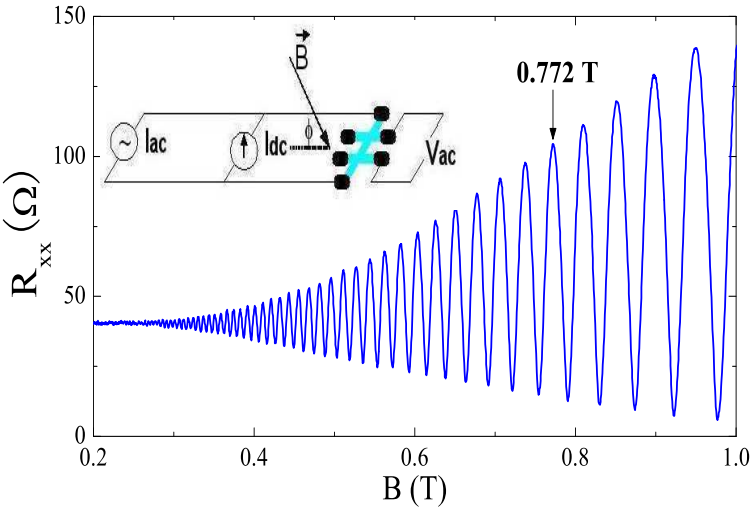

Figure 10: Quantum oscillations of the resistance at T= 1.7 K and zero dc bias for a magnetic field applied perpendicular to the electron plane(ϕ =90^o); the arrow denotes the field of the Shubnikov de Haas maximum for which subsequent data were obtained. The inset shows a schematic of the experimental set-up.

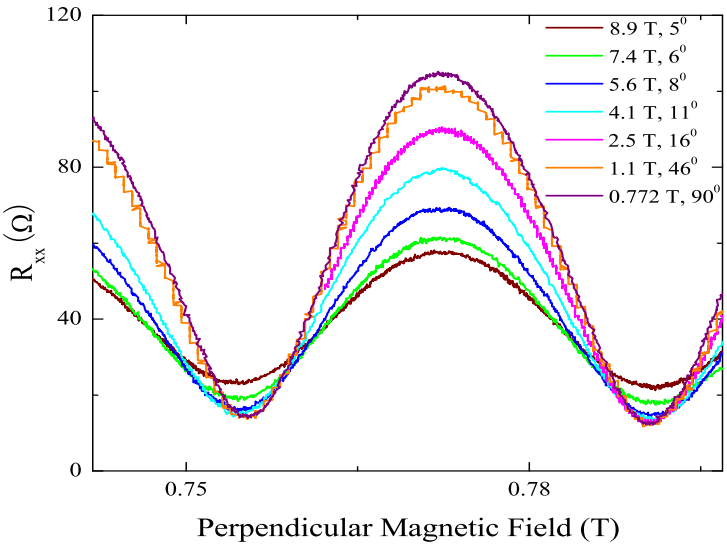

Figure 11: The resistance R_{xx} plotted as a function of the perpendicular component $B_\perp$ of the magnetic field for magnetic field applied at various angles ϕ with respect to the electron plane. The legend lists the angle ϕ and the *total* magnetic field at the maxima. Data were taken at T= 1.7 K with zero dc bias.

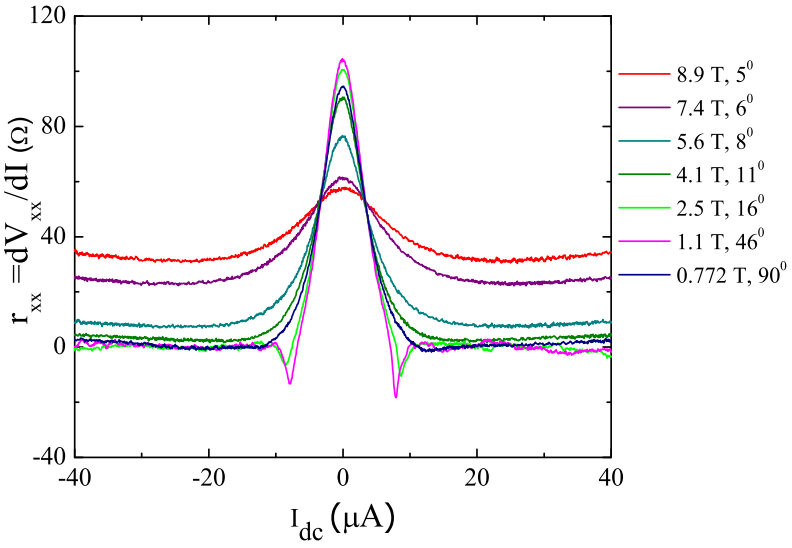

Figure 12: Differential resistance as a function of the dc bias for different angles ϕ between the magnetic field and the 2D electron plane, where the perpendicular magnetic field is $B_\perp = 0.772$ T (marked by an arrow in Fig. 10) corresponds to a SdH maximum and is fixed for all curves. Measurements were performed at a temperature T= 1.7 K.

filling factor ν is thus fixed for all curves in Fig. 11, while the Zeeman splitting $\Delta_Z = g\mu_B B$ is different for different curves due to its dependence on the total magnetic field B.

Figure 12 shows the differential resistance $r_{xx} = dV_{xx}/dI$ as a function of the dc bias at $T = 1.7$ K for different angles ϕ and fixed perpendicular magnetic field $B_\perp = 0.772$ T corresponding to the Shubnikov de Haas (SdH) oscillation maximum indicated by the arrow in Fig. 10. Note that the total magnetic field (denoted in the legend of Fig. 12) and its in-plane component both increase as the angle ϕ decreases. The differential resistance r_{xx} initially decreases with increasing bias I_{dc} for all angles. For a perpendicular magnetic field ($\phi = 90^o$) r_{xx} exhibits a reproducible negative spike at $I_{dc} = 7.9\mu$A and then stabilizes near zero. This is the zero differential resistance state. As the angle ϕ between the magnetic field and the plane is decreased, the spike gradually disappears and is no longer observable at $\phi = 21^o$. For smaller angels the differential resistance r_{xx} is increasingly positive as the angle ϕ decreases, and a shallow minimum develops at large bias.

3.4 Discussion

It is interesting to compare our results for the zero differential resistance state (ZDRS) with those reported in Ref. [31] and Ref. [32] for the effect of in-plane field on the zero resistance (ZRS) state. Both experiments were performed in magnetic fields smaller than those used in our experiments. Mani [32] tilted the sample at an angle θ with respect to the magnet axis and microwave propagation direction. The ZRS was observable with the oscillatory pattern unchanged at a tilt angle of $\theta = 80^o$ ($\phi = 90^o - \theta = 10^o$), and vanished only at $\theta \approx 90^o$. The disappearance of the ZRS at $\theta \approx 90^o$ was attributed to the vanishing of the photon flux through the two dimensional electron system rather than to the in-plane magnetic field. Yang et al. [31] employed a

two axis system to provide perpendicular and parallel field components. They report the gradual reduction of the microwave induced ZRS and its disappearance when a parallel magnetic field ($B_{||} \approx 0.5$T) is applied. Our results are qualitatively similar to those of Yang et al. [31]: we find that the ZDRS decreases and disappears gradually with increasing in-plane magnetic field component, while Mani [32] reported quenching of the ZRS only at $\theta \approx 90^o$. It is possible, however, that stronger magnetic fields, comparable to those applied in our experiments, are required to reduce the dc induced nonlinearity for $\theta < 90^o$.

We suggest that the suppression of the nonlinear response of the system and the disappearance of the zero differential resistance at small angles ϕ are due to the change of the bias-stimulated spectral diffusion of the electrons [22, 25, 27] caused by the increase of the in-plane magnetic field component. We consider Zeeman splitting of the Landau levels as the main mechanism leading to a decrease of the variations of the spectral diffusion with energy and, thus, to the reduction of the nonlinearity. Below we compare numerical simulations of the spectral diffusion with the experiment. We found good agreement between this theory and the experimental results.

To estimate quantitatively the effect of Zeeman splitting on the spectral diffusion we begin by analyzing the change in the electron spectrum induced by the Zeeman effect. As the angle of the applied magnetic field is tilted away from the perpendicular and the total magnetic field is increased, the oscillations of the density of states (DOS), $\nu(\epsilon)$, split into spin up and spin down components, as seen in Eq.(54). This leads to a reduction in the modulation of the DOS amplitude [33]. In order to calculate the DOS we use a gaussian approximation given by [34]

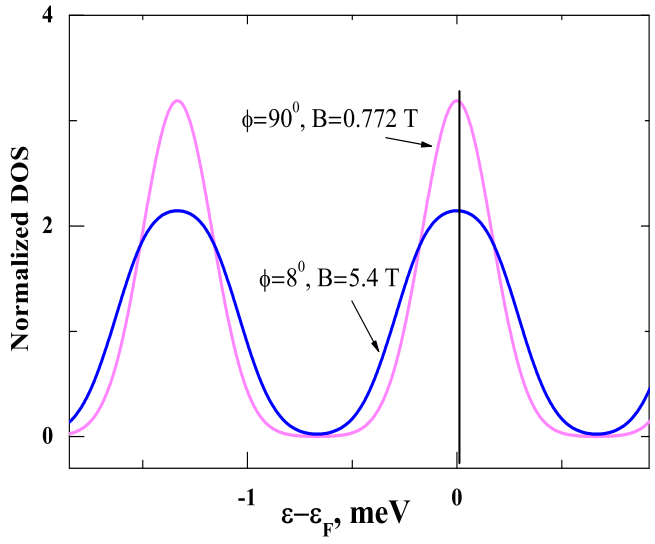

Figure 13: The density of electron states (normalized to its value at zero magnetic field) as a function of energy in a fixed perpendicular magnetic field $B_\perp = 0.772$ T and different total magnetic fields, $B = 0.772$ T at 90^o, and $B = 5.4$ T at 8^o.

$$\tilde{\nu}(\epsilon) = \frac{\nu(\epsilon)}{\nu_0} = \frac{\sqrt{\omega_c \tau_q}}{2}\left(exp\left(-\frac{(\epsilon/\hbar + \Delta_z/\hbar - n\omega_c)^2}{\omega_c/\pi\tau_q} \right) + exp\left(-\frac{(\epsilon/\hbar - \Delta_z/\hbar - n\omega_c)^2}{\omega_c/\pi\tau_q} \right) \right), \tag{54}$$

where $\tilde{\nu}(\epsilon)$ is the dimensionless DOS normalized by the value of the DOS at zero magnetic field, n is an integer, τ_q is the quantum or single particle relaxation time and ω_c is the cyclotron frequency. The parameter $\hbar/\tau_q$ determines the width of the Landau levels and is obtained from comparison with experiment (shown below). A similar value of $\hbar/\tau_q$ is also found by comparison of the experiment with the self consistent Born approximation of the density of states [35].

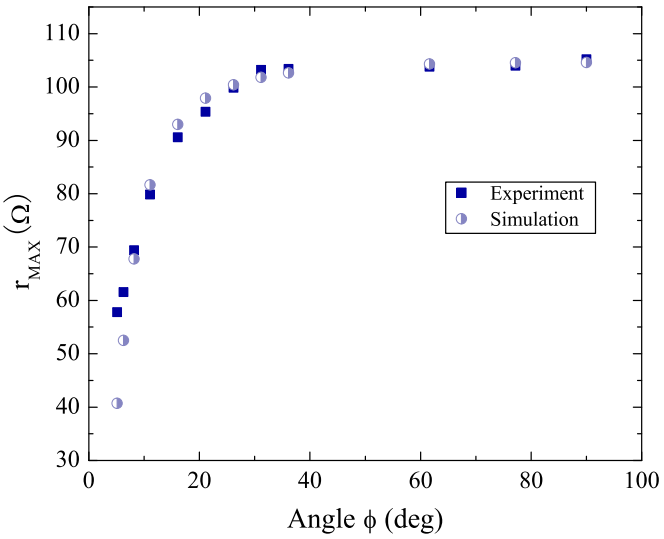

Figure 14: The differential resistance r_{MAX} of the quantum oscillation maximum at $B_\perp = 0.772$ T plotted as a function of the angle ϕ between the total magnetic field and the electron plane. The squares are the experimental results and the circles represent the numerical simulation.

The inset to Fig. 13 shows the results of the numerical simulation of the effect of Zeeman splitting on the density of electron states (DOS) in our sample. It can be seen that the modulation of the DOS is weaker for smaller angles ($\phi = 8^o$) corresponding to stronger Zeeman spin splitting.

Figure 14 presents the angular dependence of the maximum value of the differential resistance $r_{xx} = dV_{xx}/dI$ at $B_\perp = 0.772$ T obtained from the curves presented in Fig. 11. At fixed filling factor the resistance decreases with decreasing angle ϕ (with a consequent increase of the total magnetic field applied). Based on the evolution of the density of states displayed in Fig. 13, the theoretically expected values of resistance are denoted in Fig. 14 for comparison. The resistance was estimated using the simplified expression for the longitudinal conductivity in strong magnetic fields ($\omega_c \tau_{tr} \gg 1$) (see

Eq.(45)): [22]

$$\sigma_{xx} = A \times \int \sigma(\epsilon)(-df/d\epsilon)d\epsilon, \tag{55}$$

where $\sigma(\epsilon) = \sigma_D \tilde{\nu}(\epsilon)^2$, $\sigma_D = e^2\nu_0 v_F^2/2\omega_c^2\tau_{tr}$ is the Drude conductivity in a perpendicular magnetic field $B_\perp$. The free parameter A accounts for possible memory effects [29] and other deviations from Drude behavior in the presence of strong magnetic fields [36]. The parameters A and τ_q (the quantum scattering time), were chosen to provide a good fit between experiment and theory for the angular dependence of the resistance at $B_\perp = 0.772$ T. From the comparison above, we obtain the electron g-factor, $g = -0.475$, which is very close to values obtained in other experiments [37]. From the results obtained from this comparison (see Fig. 14) we find good agreement between experiment and theory. Thus, we are able to attribute the decrease of the SdH maxima with increasing in-plane magnetic field component to the Zeeman effect. In order to estimate how the electron spectral diffusion and the nonlinearity of the 2D electron system in the presence of a magnetic field is affected by the Zeeman effect, we solve numerically the spectral diffusion equation for the electron distribution function $f(\epsilon)$ (see Eq.(50)): [22]

$$-\frac{\partial f(\epsilon)}{\partial t} + E_{dc}^2 \frac{\sigma_{dc}^D}{\nu_0 \tilde{\nu}(\epsilon)} \partial_\epsilon \left[\tilde{\nu}^2(\epsilon)\partial_\epsilon f(\epsilon)\right] = \frac{f(\epsilon) - f^0(\epsilon)}{\tau_{in}}, \tag{56}$$

where $f^0(\epsilon)$ is the Fermi distribution and E_{dc} is the bias-induced electric field. For the normalized DOS, $\tilde{\nu}(\epsilon)$, we use the DOS obtained above from a comparison with the linear response (see Eq.(54), Eq.(55) and Fig. 14). We use the inelastic relaxation time τ_{in} as a fitting parameter. The solution of the diffusion equation $f(\epsilon)$ at $t \gg \tau_{in}$ is then inserted into Eq.(55) in order to obtain the resistivity at different dc biases. Figure 19 shows experimental and numerical results for the longitudinal resistance

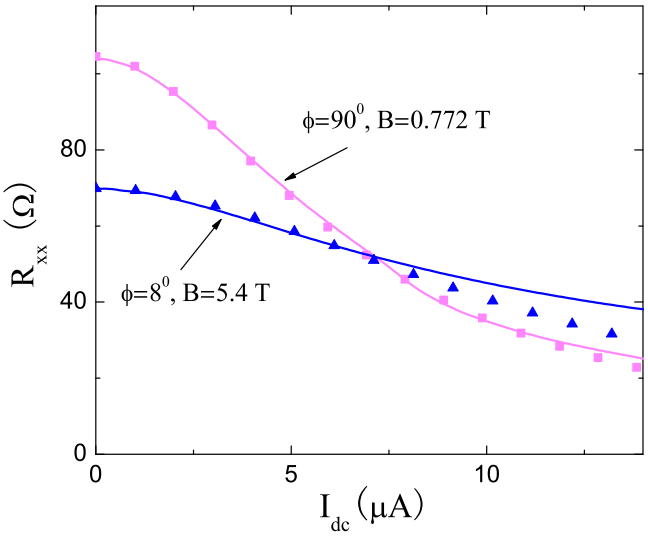

Figure 15: The solid curves show the measured resistance $R_{xx} = V_{xx}/I_{dc}$ as a function of dc bias in fixed perpendicular magnetic field for two different total magnetic fields (angles ϕ), as labeled; T= 1.7 K. The symbols denote the numerical solution of the spectral diffusion equation; $\tau_q = 5.1$ ps; $\tau_{in} = 2.6$ ns at $\phi = 90^o$ and $\tau_{in} = 2.7$ ns at $\phi = 8^o$.

R_{xx}=V_{xx}/I as a function of the dc bias plotted for two different angles, $\phi = 90^o$ and $\phi = 8^o$. The vertical scale is fixed by the comparison with the linear response (by the choice of the two parameters A an τ_q in Eq.(54) and Eq.(55)). The horizontal scale is chosen to provide the best fit between theory and experiment. The best result is obtained for the inelastic time $\tau_{in} = 2.6 \times 10^{-9}$ sec at $\phi = 90^o$ and for $\tau_{in} = 2.7 \times 10^{-9}$ sec at $\phi = 8^o$. There is good agreement between theory and experiment at small dc bias. At higher dc bias deviations become evident that are larger for smaller angles ϕ. We suggest that these deviations are due to additional nonlinear mechanisms that occur at higher dc bias [29, 38] which have not been treated in our work.

3.5 Summary

The effect of a dc electric field on the longitudinal resistance of a highly mobile two-dimensional (2D) electron system in GaAs quantum wells was studied. In our experiment we observed a zero-differential resistance state in response to a direct current when the magnetic field is perpendicular to the electron plane. At fixed filling factor the nonlinearity of the 2D electron system decreases and the zero differential resistance state disappears gradually as the total magnetic field is increased and tilted toward the 2D plane. Numerical simulations of the spectral diffusion in the presence of Zeeman splitting of the DOS in a high magnetic field provide a good fit to our experimental observations.

4 Warming in systems with a discrete spectrum: spectral diffusion in two dimensional electron systems in the presence of a magnetic field

4.1 Introduction

It is well known that application of an electric field to conductors heats electric charge carriers. Often an elevated electron temperature results from the heating of the carriers. When an electric field is applied to a conductor with a discrete electron energy spectrum, a non-equilibrium electron distribution is created. In this work [3], it is demonstrated that this non-equilibrium electron distribution cannot be described by an elevated temperature. Such electron distribution changes significantly the conductivity of highly mobile two dimensional electron systems in a magnetic field, forcing them into a state with a zero differential resistance. Most importantly the results demonstrate that, in general, the effective overheating in systems with a discrete spectrum is much stronger than the overheating in systems with continuous and homogeneous distribution of the energy levels at the same input power.

The energy distribution of hot electrons in response to an electric field is a long-standing, interesting problem in condensed matter and plasma physics [39]. Despite the simplicity of the experiments, interpretation of results is based significantly on theoretical suggestions. It is widely accepted that the behavior of overheated, degenerate electron systems is well described by an elevated electron temperature T_e. This approach is based on an analysis of the Fokker-Plank type equation with almost elastic scattering [40]. The temperature broadening of the electron distribution function affects the kinetic properties of electron systems with a discrete energy spectrum, in particular, electrons in a magnetic field. It was shown by L.D. Landau [41] that

a quantization of the electron motion in a magnetic field results in a discrete energy spectrum of the electrons (see section 1.2.3). Direct consequences of this Landau quantization are quantum magnetic oscillations in metals: the Shubnikov de Haas effect (see section 1.2.2) and the de Haas-van Alphen effect [42, 43]. At thermal equilibrium the amplitude of the quantum oscillations depends exponentially on the electron temperature T_e, and often these oscillations are used as an electron thermometer.

4.2 Experimental Setup

Our samples are cleaved from a wafer of a high-mobility GaAs quantum well grown by molecular beam epitaxy on semi-insulating (001) GaAs substrates. The width of the GaAs quantum well is 13 nm. Three samples (N1,N2,N3) are studied with electron density n_1=8.2 $\times 10^{15}$ m^{-2}, n_2=8.4$\times 10^{15}$ m^{-2}, n_3=8.1$\times 10^{15}$ m^{-2} and mobility μ_1=85 m^2/Vs, μ_2=70 m^2/Vs and μ_3=82 m^2/Vs at T = 2 K. Measurements were carried out between T = 0.3 K and T = 10 K in magnetic fields of up to 1.5 T. The measurements were performed on d=50 μm wide Hall bars with a distance of 250 μm between potential contacts. The differential longitudinal resistance was measured at a frequency of 77 Hz in the linear regime. Direct electric current (dc bias) was applied simultaneously with ac excitation through the same current leads (see inset to Fig. 16). All samples demonstrate similar behavior. Below we present data for sample N1.

4.3 Experimental Results

Figure 16(a) shows the longitudinal resistance $r_{xx} = dV_{xx}/dI$ [44] as a function of the magnetic field B at zero DC bias and at different temperatures as labeled. At B >0.4 T the resistance exhibits the Shubnikov de Haas oscillations. The amplitude of the oscillations decreases significantly with the increase in temperature. The decrease of

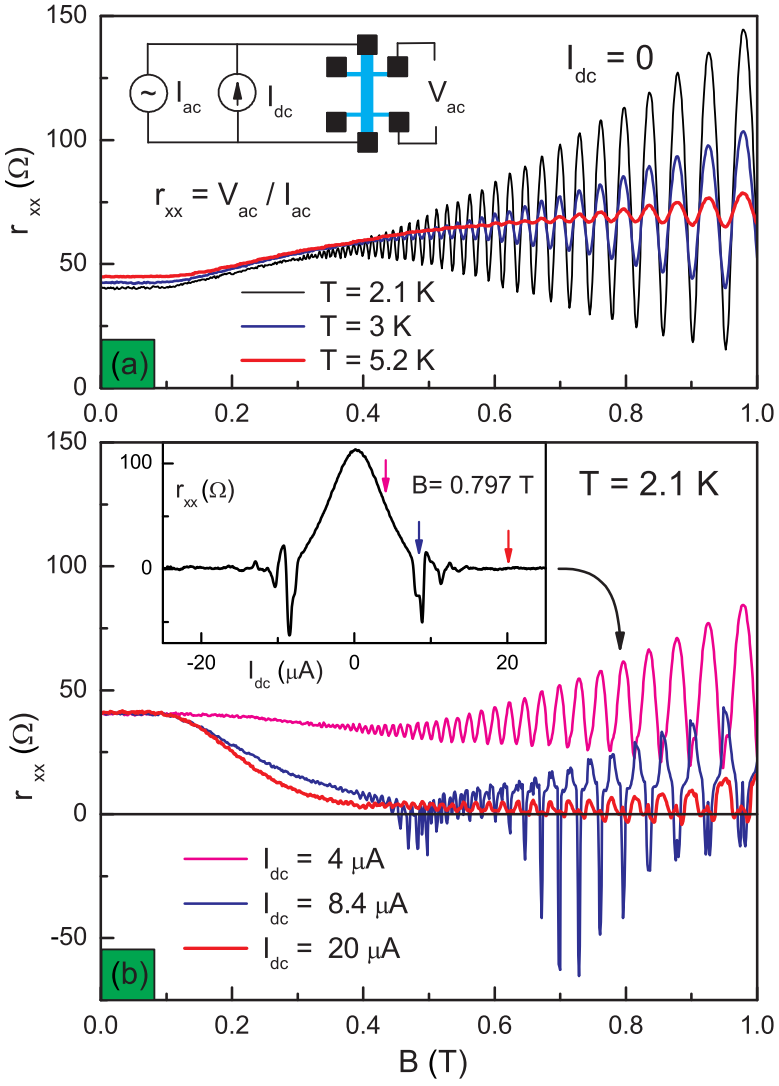

Figure 16: (a) Dependence of the longitudinal resistance r_{xx} on magnetic field B with no *dc* bias I_{dc} applied at different temperatures as labeled. The inset presents the experimental setup. (b) Dependence of the longitudinal resistance r_{xx} on magnetic field B at different *dc* bias I_{dc} as labeled. The inset presents the bias dependence at fixed magnetic field B=0.797 T. Measurements were taken at $T = 2.1$ K.

the SdH amplitude with temperature increase is a result of an effective (exponential) cancellation of the periodic oscillations of the electron conductivity $\sigma(\epsilon)$ with energy ϵ weighted with the first derivative of the equilibrium (Fermi-Dirac) distribution function $df/d\epsilon$ and averaged over all possible energies [43] (see Eq.(45)):

$$\sigma = \int \sigma(\epsilon)(-df/d\epsilon)d\epsilon \tag{57}$$

Figure 16(b) shows the longitudinal resistance $r_{xx} = dV_{xx}/dI$ as a function of the magnetic field B taken at three different dc biases as labeled at a lattice temperature $T = 2.1$ K. The dc electric field changes significantly the longitudinal resistance in magnetic fields above 0.15 T. At $B > 0.15$ T the disorder broadening $\hbar/\tau_q$ of the Landau levels is less than the Landau level separation $\hbar\omega_c$ and the electron energy spectrum (density of states) becomes modulated. The modulation increases with the magnetic field. At $B \sim 1$ T the Landau levels are completely separated from each other and the electron spectrum is discrete.

The inset of Fig. 16(b) demonstrates a typical dependence of the longitudinal resistance r_{xx} on the dc bias in a magnetic field ($B = 0.797$ T), corresponding to an oscillation maximum. For small dc biases the resistance decreases approaching zero. As the dc bias is raised further, the resistance exhibits a reproducible sharp negative spike at I_{th}=8.4 μA and, then, stabilizes near zero at higher biases. This is the zero differential resistance state, and it was observed in a broad range of magnetic fields and at temperatures below a few Kelvins[27, 28].

4.4 Discussion

The curves presented in Fig. 16(b) reveal an unexpected evolution of the SdH oscillations with the dc bias. The behavior is significantly different from the temperature

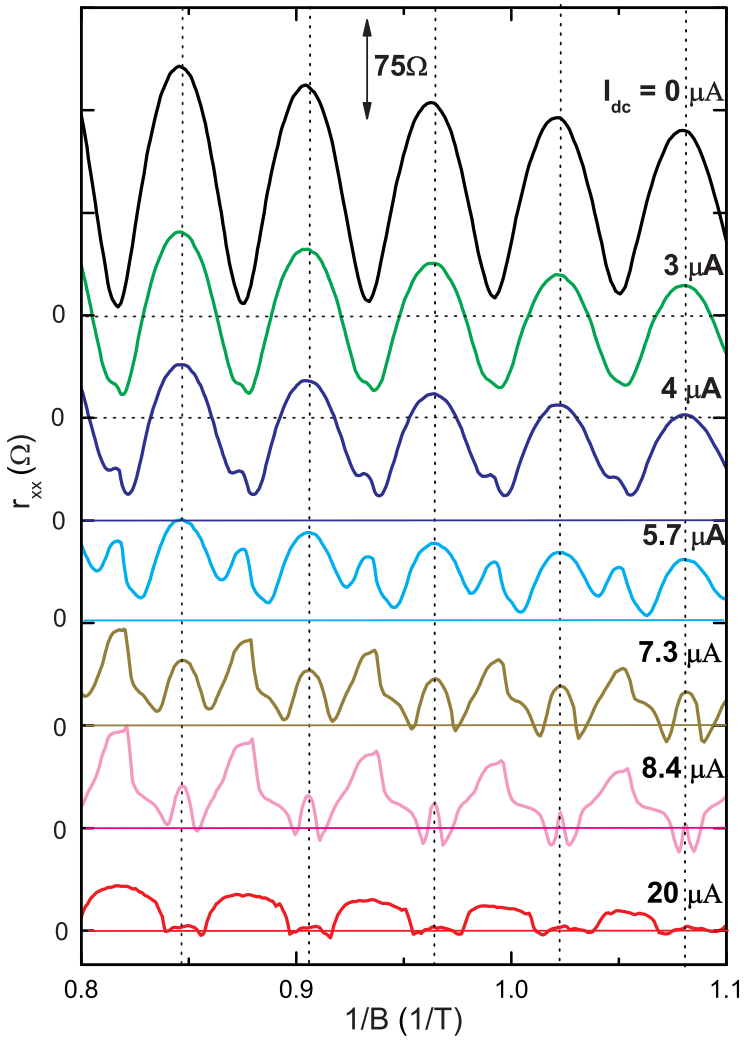

Figure 17: The longitudinal resistance r_{xx} plotted as a function of the inverse magnetic field $1/B$ at different *dc* biases, as labeled. Measurements were taken at $T = 2.1$ K.

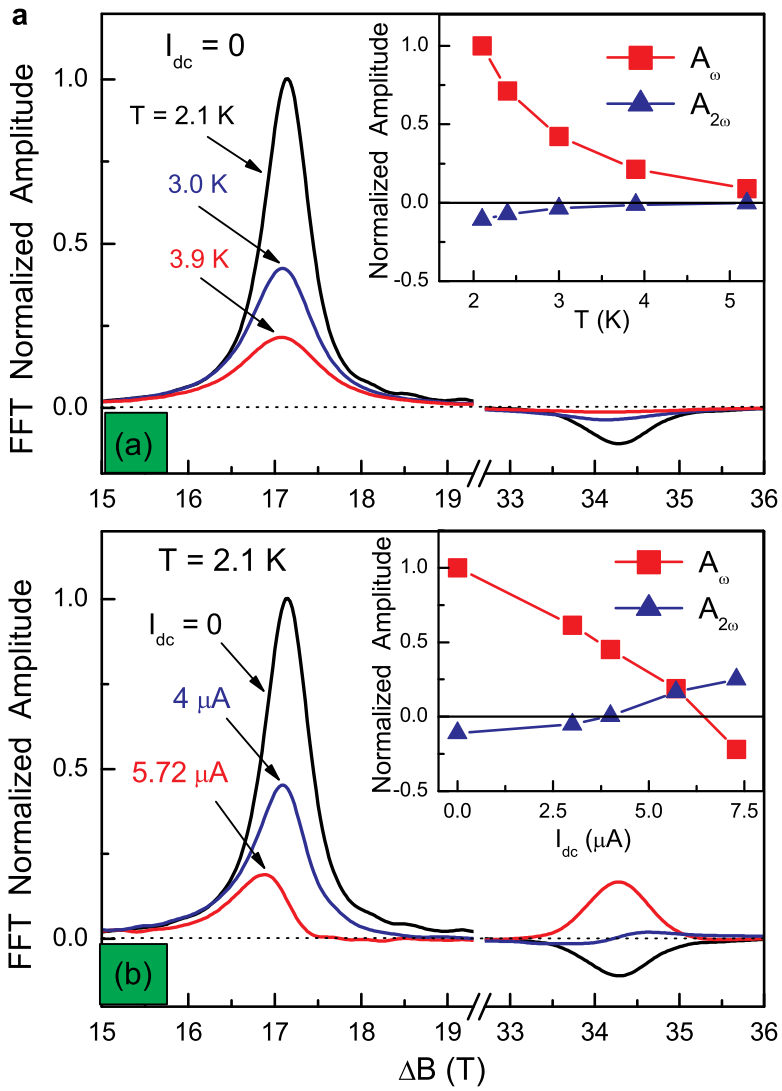

Figure 18: (a) Fourier spectrum of the quantum oscillations at different temperatures as labeled. Insert shows temperature dependence of amplitude of first (at 17.1 T) and second (at 34.2 T) harmonics of the quantum oscillations. Zero *dc* bias. (b) Fourier spectrum of the quantum oscillations at different *dc* bias as labeled. In the inset shows the bias dependence of amplitude of first (at 17.1 T) and second (at 34.2 T) harmonics of the quantum oscillations. The lattice temperature is 2.1 K.

evolution shown in Fig. 16(a). Both oscillating and smooth parts of the dependences in Fig. 16(b) exhibit substantial changes. The smooth part of the resistance displays a strong reduction with the *dc* bias in magnetic fields $B > 0.15$ T, at which the density of electron states oscillates with energy. The oscillating part of the resistance reveals a rather complicated behavior with the *dc* bias.

Figure 17 presents the bias induced evolution of the quantum oscillations in greater detail. The oscillations are periodic when plotted as a function of the inverse magnetic field $1/B$ [42]. Although the fundamental periodicity is the same for all biases, the form of the oscillations and the harmonic content change significantly with the dc bias. The most visible changes occur at maxima of the oscillations. With the increasing bias the maxima evolve gradually into minima with essentially zero differential resistance. On the other hand the minima tend to form maxima and, finally, separate the zero resistance regions at the end of the evolution. For further discussion it is important to realize that the high frequency content of the oscillations with respect to the fundamental periodicity increases when the *dc* bias is increased.

Figure 18(a) demonstrates quantitatively the evolution of the first and second harmonics of the quantum oscillations with temperature at zero dc bias. At thermal equilibrium the distribution function f does not oscillate with energy and, therefore, the harmonic content of the quantum oscillations is determined *only* by the harmonic content of the conductivity $\sigma(\epsilon)$ oscillating with energy ϵ due to Landau quantization. The amplitudes of the first $A_\omega(T)$ and the second $A_{2\omega}(T)$ harmonics exhibit exponential decrease with the temperature due to the spectral average of the oscillations of the conductivity $\sigma(\epsilon)$ over the range of energies $\Delta\epsilon$ corresponding to the thermal broadening of the distribution function $\Delta\epsilon \sim kT$. At higher frequency the spectral cancellation is more effective and, as a result, the higher harmonics of the quantum oscillations ($A_{2\omega}(T)$) are exponentially smaller than the amplitude of the fundamental

periodicity $A_\omega(T)$. The inset of Fig. 18(a) demonstrates that the amplitudes of the first A_ω and the second $A_{2\omega}$ harmonics as well as their ratio $R = A_{2\omega}/A_\omega$ decrease significantly with the temperature and approach the zero value asymptotically.

Figure 18(b) demonstrates the effect of the *dc* bias on the spectrum of the quantum oscillations. Notably different behavior of the first and especially the second harmonics with *dc* bias is observed. The first (fundamental) harmonic does not approach the zero value asymptotically. Instead, as it is shown on the inset of Fig. 18(b), the amplitude crosses the zero value and becomes negative at $I_{dc} = 7.5$ μA. In other words, the phase of the fundamental oscillations changes by 180^0. This corresponds to the evolution presented in Fig. 17(b), where maxima become minima with the bias increase. Even more unusual is the behavior of the second harmonic of the oscillations. One can see that the magnitude of second harmonics does not exponentially decrease with the *dc* bias contrary to the usual expectation. Instead the second harmonic crosses the zero and reaches a value, which is even bigger than the amplitude $A_{2\omega}(0)$ at zero bias. At the same time, the ratio R between the amplitudes of the second and first harmonics is on the order of unity, which, again, cannot be explained by the temperature broadening of the distribution function. Thus the results indicate that the effect of the direct current on the resistance of a 2D electron system with a discrete energy spectrum cannot be explained by an increase of the electron temperature.

The enhancement of the higher harmonics of the quantum oscillations with the dc bias follows directly from Eq.(57) assuming additional, bias induced *oscillations* of the non-equilibrium distribution function with the energy. Such oscillations have been found theoretically in dc biased 2D electron systems recently[22].

The spectral diffusion equation [22] is solved numerically:

$$-\frac{\partial f(\epsilon)}{\partial t} + E_{dc}^2 \frac{\sigma_{dc}^D}{\nu_0 \tilde{\nu}(\epsilon)} \partial_\epsilon \left[\tilde{\nu}^2(\epsilon) \partial_\epsilon f(\epsilon) \right] = \frac{f(\epsilon) - f^0(\epsilon)}{\tau_{in}}, \tag{58}$$

Results of the numerical simulation of the spectral diffusion are shown in Fig. 19(a). As expected the spectral diffusion produces periodic variations of the distribution function $f(\epsilon)$ with energy.

4.5 Summary

It is clear, that an elevated temperature T_e cannot describe this oscillating behavior. The additional oscillations of the distribution function enrich significantly the harmonic content of the product $\sigma(\epsilon)(-df/d\epsilon)$ and, therefore, in accordance with Eq.(57), the spectrum of the quantum oscillations. Furthermore, as shown in Fig. 19(b), the considerable decrease of the value $df/d\epsilon$ at the maxima of the conductivity $\sigma(\epsilon)$ (and the maxima of the density of states) makes the net conductivity σ significantly smaller than the unbiased value. This explains the strong reduction of the conductivity (and resistivity r_{xx} [44]) with the DC bias at magnetic fields $B > 0.15$ T shown in Fig. 16(b).

The strong reduction of the gradient of the electron distribution function $df(\epsilon)/d\epsilon$ near the maxima of the conductivity $\sigma(\epsilon)$ and the density of states imitates strong overheating in these energy regions. Indeed, Fig. 19(b) demonstrates that at a maximum of the density of states located at the Fermi level μ: $\epsilon - \mu = 0$, the gradient of the DC biased distribution function $df(\epsilon)/d\epsilon$ is equal to the gradient of the distribution function corresponding to thermal equilibrium at a temperature of 32 K. Thus, at the conductivity maximum $\sigma(\epsilon = \mu)$ the effective overheating of the 2D electron system (32 K) is significantly stronger than the actual additional broadening of the distribution function ($\sim 1 - 2K$) induced by the dc bias. This provides the significant change in the transport properties of the system (see Fig. 16(b)).

The strong reduction of the $df/d\epsilon$ is a result not only of the high spectral diffusion near the spectral maxima, but mostly a result of the *weak* spectral diffusion between

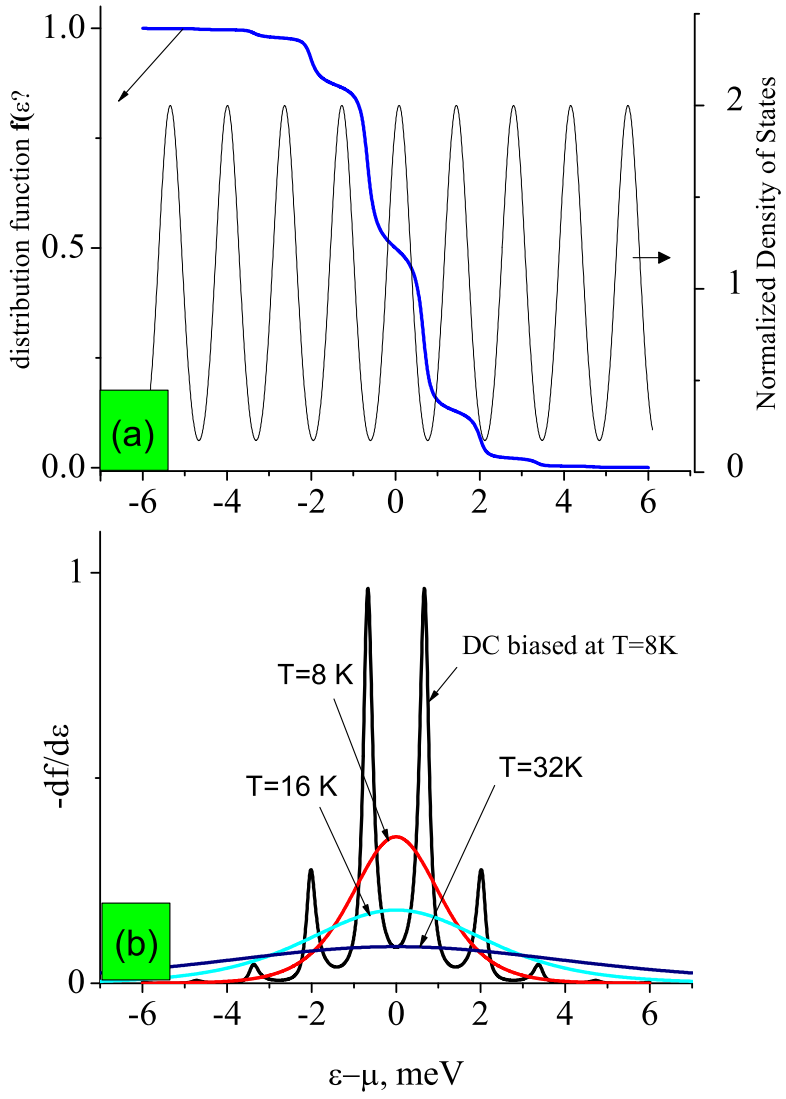

Figure 19: (a) right axes: density of states of the electrons in a magnetic field $B = 0.797$ T as a function of energy; left axes: numerical calculations of the electron distribution function modified by the electron spectral diffusion. The following parameters are used in the simulation: magnetic field $B = 0.797$ T, temperature $T = 8$ K, *dc* electric field $E_{dc} = 1003$ V/m, disorder broadening of Landau levels $\hbar/\tau_q$=$\hbar$/1.9 1/ps and inelastic scattering time $\tau_{in} = 150$ ps. The times are obtained by comparison with experimental results; (b) The gradient $df/d\epsilon$ of the distribution function modified by the spectral diffusion shown above and the gradient of the thermal equilibrium function corresponding to different temperatures as labeled.

them. In fact, the weak diffusion between the spectral maxima controls the overall spectral flow J_ϵ. In some sense, the regions of phase space with weak spectral diffusion provide "thermal" isolation from the regions with strong spectral diffusion. This dc bias induced, thermal stratification of phase space facilitates strong overheating in the regions essential for the net electron transport.

Spectral diffusion and thermal stratification are also expected in 2D electron systems in the presence of electromagnetic radiation. In this case spectral diffusion is a result of quantum transitions between energy levels induced by the external radiation. This points toward a generic nature of the phenomena. The presented results suggest that in systems with a discrete or strongly modulated energy spectrum the effective overheating is significantly *stronger* than the one in systems with a weakly modulated homogeneous spectrum at the same input power.

5 Two-parameter scaling of microwave rectification vs microwave power at the boundary between two-dimensional electron systems

5.1 Introduction

In two-dimensional systems of electrons, at high magnetic fields, and in response to microwave radiation and DC bias, strongly nonlinear transport [2, 11, 12, 15, 16, 17, 18, 20, 21, 22, 23, 24, 25, 26, 38, 45, 46, 47, 48, 49] that gives rise to unusual states [13, 14, 27] has been reported. There has also been great interest in the nonlinear response of quantum ballistic constrictions, where the effects of quantum interference, spatial dispersion and electron-electron interactions play crucial roles [50, 51, 52, 53, 54, 55, 56, 57, 58, 59, 60, 61].

In this work [4] we report a new type of nonlinearity of thermoelectric origin in a two-dimensional system of electrons. We have investigated the rectified (DC) voltage induced by microwave radiation applied locally to the boundary between two-dimensional electron systems with different electron densities n_1 and n_2. A simple experimental geometry is used in which closely spaced, electrically isolated gates give rise to a very large microwave field localized at the narrow slit between the gates, thereby enhancing the nonlinear response in the immediate vicinity of the gap. The gates are used to vary the electron densities separately and independently, providing a convenient and effective tool to control the strength of the nonlinearity. The rectified voltage V_{dc} is found to be an odd function of the difference $\Delta n = n_2 - n_1$ between the electron densities n_1 and n_2 of the two systems. Using two scaling parameters, all the data above 4 GHz taken at different temperatures can be collapsed onto a single universal curve.

Excellent quantitative agreement is obtained with a theory that considers the local overheating of the electrons by microwaves near the narrow boundary between the 2D systems, which gives rise to a voltage through the thermoelectric effect between two dissimilar two-dimensional metals. A fit of the experimental data to this theory yields an electron-phonon coupling constant that is in reasonable agreement with the coupling constant obtained by a recent theory [62] as well as other experiments [63].

This experimental protocol provides an effective method for studying the thermoelectric properties of low dimensional systems. An important advantage relative to other approaches [63] is that the electron system is heated directly by the microwaves with negligible heating of the phonon system, thereby reducing the contribution of phonon drag to the thermoelectricity. This work is a continuation and expansion of research reported earlier [65, 66].

5.2 Theory of microwave rectification in two 2D electron systems

In this section we present a quantitative theory for the microwave rectification in two 2D electron systems. In this theory the DC voltage results from the thermoelectric effect induced by local microwave overheating of the area near the boundary between two dissimilar 2D electron metals. First we present a system of electrodynamic equations, which allows us to find the distribution of microwave electric potential across the sample. We will show that at high frequency the microwave field is localized near the narrow gap between the metals. Then we solve the thermoconductivity equation assuming fast thermalisation of hot 2D electrons and find the temperature profile inside the electron system. Deviations from the isotropic Fermi distribution should not significantly affect the spatial relaxation. The thermoelectric voltage V_{dc} is found by

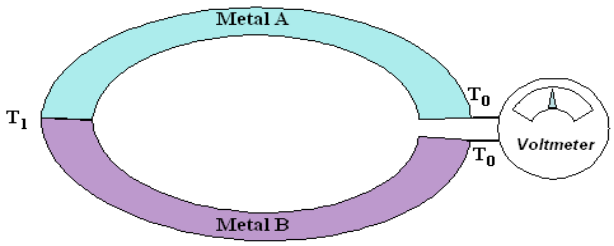

Figure 20: Circuit for measuring the difference in the thermoelectric voltages which develop in two different metals, where in each of them the temperature varies from T_0 to T_1.

direct integration of the thermoelectric field across the sample.

5.2.1 The Thermoelectric effect

When a temperature gradient [9] is maintained in a metal and no electric current is allowed to flow, there will be a steady-state electrostatic potential difference between the high and low temperature regions of the specimen. Such a circuit is depicted in Fig. 20. The voltmeter in Fig. 20 connects points of the specimen at the same temperature, otherwise there would be a temperature gradient in the circuit of the meter itself, which would create an additional thermoelectric voltage. Since no thermoelectric voltage develops between points of a single metal at the same temperature, the circuit used is of two different metals connected such that one is at temperature T_1 and the other at a temperature $T_0 \neq T_1$. This measurement yields the difference in the thermoelectric voltages developed in the two metals.

The electric field that we measure is directed opposite to the temperature gradient.

This field is the thermoelectric field, and it is given by

$$\mathbf{E}' = Q(T)\nabla T \tag{59}$$

The current is driven not just by the electric field $\mathbf{E}$, but by $\mathbf{E}' = \mathbf{E} + \frac{\nabla\mu}{e}$, where μ is the chemical potential. This is because the chemical potential gradient leads to a diffusion current. $Q(T)$ is the thermopower coefficient of a metal. We may obtain $Q(T)$ is by considering the current density given by

$$\mathbf{J} = 2\int e\mathbf{v}f d\mathbf{k} \tag{60}$$

the electron distribution function f in the presence of a uniform static electric field and a temperature gradient is given by

$$f = \tau\frac{\partial f}{\partial\epsilon}\mathbf{v}\cdot\left[-e\mathbf{E}' + \frac{\epsilon-\mu}{T}(-\nabla T)\right] + f^0 \tag{61}$$

we may therefore write the electrical current density as

$$\mathbf{j} = L_1\mathbf{E}' + L_2\ (-\nabla T). \tag{62}$$

Since negligible current flows when the thermoelectric voltage is measured, we obtain

$$Q(T) = \frac{L_1}{L_2}. \tag{63}$$

In the treatment below, the thermopower coefficient is given by $Q(T) = \frac{1}{3}\pi^2 T/(eE_F)$.

5.2.2 Derivation of the dependence of the rectified voltage V_{dc} on the microwave power P

In the derivation of the microwave (ac) current distribution, we take into account (i) that the microwave wavelength ($0.7 - 30$ cm) is much larger than the device size (~ 0.05 cm) and, therefore, we can omit the term $\partial B/\partial t$ in Maxwell's equations; and (ii) that the scale at which the electric potential varies l_{ac} is much larger than the effective distance of the 2D conducting layer from the gates d. Together with the law of electric charge conservation, the full set of equations for the time-dependent current distribution $j(x,t)$, density $\delta n(x,t)$, and the electric potential at the 2D conducting plane reads:

$$j(x,t) = \sigma(x)\nabla\phi(x,t). \tag{64}$$

$$\partial_t[e\delta n(x,t)] = -\nabla j(x) \tag{65}$$

$$\phi(x,t) = \phi_0(x,t) + \frac{ed}{\epsilon\epsilon_0}\delta n(x,t), \tag{66}$$

where $\sigma(x)$ is the local conductivity, ϵ is the dielectric constant of SiO_2 and $\phi_0(x,t) = \frac{1}{\pi}V_{ac}\arctan(x/d)\cos(\omega t)$ [67].

At high frequencies, $\omega/2\pi$ >10 GHz, the major part of the microwave power is absorbed by the 2DEG in the narrow strip under the slit between the two gates. The size of the narrow region (hot strip) is

$$l_{ac} = \left(\frac{2\sigma d}{\omega\epsilon\epsilon_0}\right)^{1/2}. \tag{67}$$

Figure 21 shows the distribution of microwave power (solid line) obtained by a numerical solution of Eqs. (64-66). The microwave power is found to be localized near the

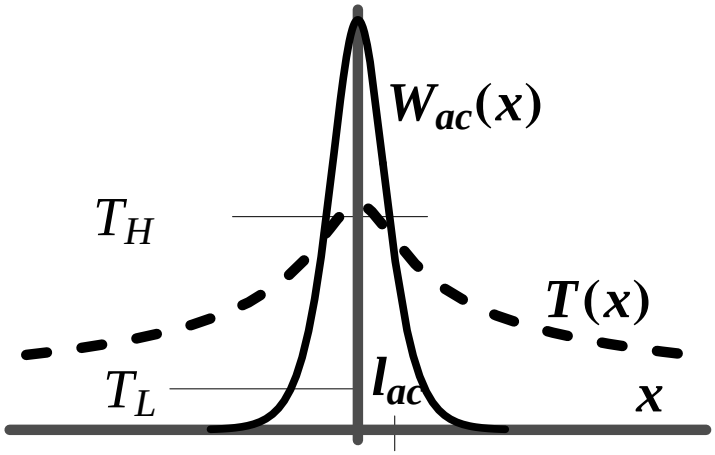

Figure 21: Joule input (solid line) and electron temperature (dashed line) *vs* distance x from the center of the hot strip

slit.

The electron temperature distribution obeys the thermoconductivity equation:

$$\nabla(\kappa\nabla T(x)) = F(T(x)) - W_{ac}(x) \tag{68}$$

where κ is thermoconductivity coefficient, $W_{ac}(x)$ is Joule heat and $F(T)$ stands for the power losses. The result of numerical integration of Eq.(68) together with Eqs. (64-66), gives a temperature distribution shown schematically in Fig. 21 by the dashed line. We use $F(T) = R(T) - R(T_L)$ for the power losses due to phonons [63], where $R(T)$ is the electron-phonon relaxation rate and T_L is the lattice temperature, which we assume to be unaffected by the microwaves. Fig. 21 shows that the Joule heat decreases exponentially from the slit as $\exp[-2x/l_{ac}]$, while the electron temperature relaxes much more slowly as $(x/L_T)^{-1/2}$.

At zero *dc* current the temperature gradient and electric field are related by (see Eq.(59))

$$E(x) = Q(T)\nabla T(x), \tag{69}$$

where the thermopower coefficient $Q = \frac{1}{3}\pi^2\beta T/(eE_F)$ with numerical coefficient $\beta \sim 1$ [64]. The electric potential difference between the two contacts is found by integrating the left and right sides of equation (69) over the distance x:

$$V_{dc} = A(T_L) \cdot (y(0) - 1) \tag{70}$$

$$A(T_L) = \frac{\pi^2 T_L^2}{6e}\left(\frac{\beta_L}{E_{FL}} - \frac{\beta_R}{E_{FR}}\right), \tag{71}$$

where we have introduced a dimensionless parameter $y(x) = (T(x)/T_L)^2$. The indexes L and R correspond to the left and right sides of the 2DEG and $T(x)$ is the temperature of the hot electrons along the sample. The coefficient A is antisymmetric with respect to the difference between Fermi energies in the left and right regions and is thus antisymmetric with respect to the difference of electron densities $\Delta n = n_R - n_L$. This behavior is consistent with the experimental observations (see Fig. 24).

At low *ac* power a small electron overheating $\Delta T = T(0) - T_L$ is proportional to the microwave power P and the linear dependence of V_{dc} on the microwave power follows from Eq.(70). In the high power regime the voltage V_{dc} is determined by the electron temperature below the slit $T(0)$ which, in turn, depends non-linearly on the microwave power. The crossover from the linear to the non-linear regime occurs at $(T(0) - T_L)/T_L \sim 1$. Note that if l_{ac} is much less than the sample size, then Eqs. (70),(71) holds independently of the model for the thermoconductivity and the power loss function $F(T)$. Therefore, the only parameter that determines the voltage V_{dc} is the temperature $T(0)$ of the 2D electrons in the hot strip under the slit.

To find the temperature profile we solve the thermoconductivity Eq.(68). Since in our setup the phonon system is not directly heated by the microwave radiation, the phonon temperature is weakly affected by the microwaves. To compare theory with the exper-

imental findings, both the phonon heat transport and the phonon drag contribution to the thermopower are neglected. To proceed further we use the Wiedemann-Franz law for the electron thermoconductivity $\kappa(T) = \pi^2\sigma T/(3e^2)$. When $x \gg l_{ac}$ we can reduce the order of the differential equation (68) by neglecting the second term on the right hand side (Joule heat) yielding

$$(\frac{\pi^2\sigma T_L^2}{12e^2})\left(\frac{dy}{dx}\right)^2 = R(T_L)(\frac{1}{4}y^4 - y + \frac{3}{4}) \tag{72}$$

Experiments [63] have shown that in the temperature range from 1 to 5 K

$$R(T) = R_1 T^6, \tag{73}$$

where R_1 is a constant. For the density $8.5\times10^{11}\mathrm{cm}^{-2}$, $R_1 \approx 1.3\,\mathrm{mW\cdot m^{-2}K^{-6}}$. According to the theory [62] $R(T)$ deviates weakly from the T^6 law and depends on electron concentration as $n^{-1/2}$. The temperature relaxation length can be expressed in terms of $\kappa(T)$ and $R(T)$ as

$$L_T = \sqrt{\frac{T\ \kappa(T)}{R(T)}}. \tag{74}$$

The total Joule heat of the 2DEG W_{ac}^T is given by

$$W_{ac}^T = \int \overline{j(x,t)\nabla\phi(x,t)dx} = \eta V_{ac}^2\left(\frac{\sigma_L}{l_{ac}^L} + \frac{\sigma_R}{l_{ac}^R}\right), \tag{75}$$

where the upper bar denotes average over time and $\eta \sim 1$ is a numerical factor.
At a stationary state the input heat is partially absorbed by the phonon system and partially drained via the electron thermal flow. When $l_{ac} \ll L_T$, most of the input power generated in the hot strip, $-l_{ac} < x < l_{ac}$, must be drained away via the thermal

electron flow, because the hot strip is much smaller than the total overheated area ($\sim L_T$) absorbing the total heat input. In this case, neglecting the phonon absorption in the hot strip area, a simple integration of Eq.(68) over the region $-l_{ac} < x < l_{ac}$ leads to:

$$W_{ac}^{T} = \frac{\pi^2 T_L^2}{6e^2}\left[\sigma_L\left(\frac{dy}{dx}\right)_L - \sigma_R\left(\frac{dy}{dx}\right)_R\right] \tag{76}$$

Combining (72), (75), (76), (67) and (85) we obtain a relation between the microwave input power P and the temperature of the 2D electrons under the slit as $y(0) = (T(0)/T_L)^2$:

$$P = B(T)\cdot\left(y(0)^4 - 4y(0) + 3\right)^{1/2} \tag{77}$$

$$B(T) = \frac{\sqrt{3}\pi}{6\eta G^2}\left(\frac{T_L^2 R(T_L) d}{e^2\omega\epsilon\epsilon_0}\right)^{1/2} \tag{78}$$

These equations, together with equation (70), determine the dependence of the rectified voltage V_{dc} on the lattice temperature T_L and microwave power P. Expanding (77) at small P we get

$$y(0) = 1 + \frac{\eta\sqrt{2}P}{\pi G^2}\left(\frac{T_L^2 R(T_L) d}{e^2\omega\epsilon\epsilon_0}\right)^{-1/2} \tag{79}$$

and for the weakly nonlinear regime ($y(0) - 1 \ll 1$)

$$V_{dc} = \frac{A(T_L)P}{\sqrt{6}B(T_L)} \sim \frac{L_T}{l_{ac}}\frac{eV_{ac}^2}{E_F} \tag{80}$$

One can see that, expressed in normalized values of the DC voltage $V_{dc}^* = V_{dc}/A(T)$ and the input microwave power $P^* = P/B(T)$, the system of equations (70) and (77)

exhibits a universal form in the whole range of microwave power:

$$V_{dc}^{*} = y(0) - 1 \tag{81}$$

$$P^{*} = (y(0)^4 - 4y(0) + 3)^{1/2} \tag{82}$$

The universal dependence V_{dc}^{*} vs P^{*} is plotted in Fig. 26, together with the scaled data points. Excellent agreement is found between the experiment and the theory in a broad range of temperature and microwave power. Random deviations between the experiment and the theory observed at low power are mostly due to low signal/noise ratio for signals below 1 μV.

To conclude the theory section we consider other mechanisms that may also lead to rectification of an *ac* voltage. We first consider the bulk rectification associated with the fact that σ in Eq.(64) may vary due to microwave modulation of the electron density and/or mobility inside the 2DEG [55, 68]. To estimate this effect we assume that the bulk rectification is due to a periodic variation of the electron density induced by the microwave modulation of the gate voltage V_g: $\delta n = n \cdot V_{ac}/V_g$ [55]. The induced *dc* current $I_{dc}^{bulk} = \sigma V_{dc}^{bulk} = \delta\sigma V_{ac}$. Therefore $V_{dc}^{bulk} = \frac{\delta\sigma}{\sigma} \cdot V_{ac} = \frac{\delta n}{n} \cdot V_{ac} = V_{ac}^2/V_g$. This is considerably smaller than the rectification due to the thermoelectric effect: From Eq.(80), $V_{dc} \sim V_{ac}^2/E_F$, as $E_F \ll V_g$. Comparison of V_{dc}^{bulk} with result (80) shows that $V_{dc}^{bulk} \sim 2 \cdot 10^{-4} V_{dc}$.

Another possible mechanism of rectification is related to the spatial variation of the electron density across the boundary [69]. Due to this variation there is a diffusive electron flow through the boundary. The net flow of electrons must be zero at thermodynamic equilibrium. An internal electric field E_b is established to compensate the diffusive flow across the boundary creating a so-called contact potential difference. Microwave radiation moves the electron system away from thermodynamic equilib-

rium. The non-equilibrium (symmetric) part of the distribution function is driven by the internal electric field E_b creating a rectified current and rectified voltage V_{dc}^b. This voltage is estimated to be [69]: $V_{dc}^b \sim \tau^2 e/m \cdot ln(n_1/n_2) \cdot E_\omega^2$, where τ is the relaxation time, assumed in [69] to be on the same order of magnitude as the transport relaxation time, m is the band mass of the 2D electrons, and $E_\omega \sim V_{ac}/l_{ac}$ is the ac electric field near the boundary. Using our result for l_{ac} we get

$$V_{dc}^b \sim \frac{1}{en_{1,(2)}d}\tau\omega V_{ac}^2 \cdot ln(n_1/n_2). \tag{83}$$

Comparison of V_{dc}^b with (80) shows that $V_{dc}^b \sim 5 \cdot 10^{-4} V_{dc}$, and is inconsistent with the significant temperature dependence observed in the experiment.

5.3 Experimental Procedure

The high-mobility Si-MOSFETs ($\mu = 2$ m^2/(Vs) at $T = 4$ K, $n = 5 \times 10^{15}$ m^{-2}) used in these studies are equipped with several metallic gates that can be separately controlled. A narrow split obtained by reactive ion etching separates the different gates. Each 2D electron system is formed below a rectangular $50 \times 240 \mu$m^2 gate by the application of a positive voltage (see Fig. 22(A)). The typical slit width of $50-70$ nm is less than the thickness of the Si oxide insulating layer (152 nm), providing a smooth variation of the electron density between the two electron systems formed below the gates, as shown in Fig. 22(B). For a slit width, w, that is much smaller than the distance d between the gates and the 2DEG, the profile of electron density is given by [71]:

$$n(x) = \frac{n_1 + n_2}{2} + \frac{n_1 - n_2}{2} \tanh(\frac{\pi x}{d}), \tag{84}$$

where x is the distance from the center of the slit. For the actual parameters of our

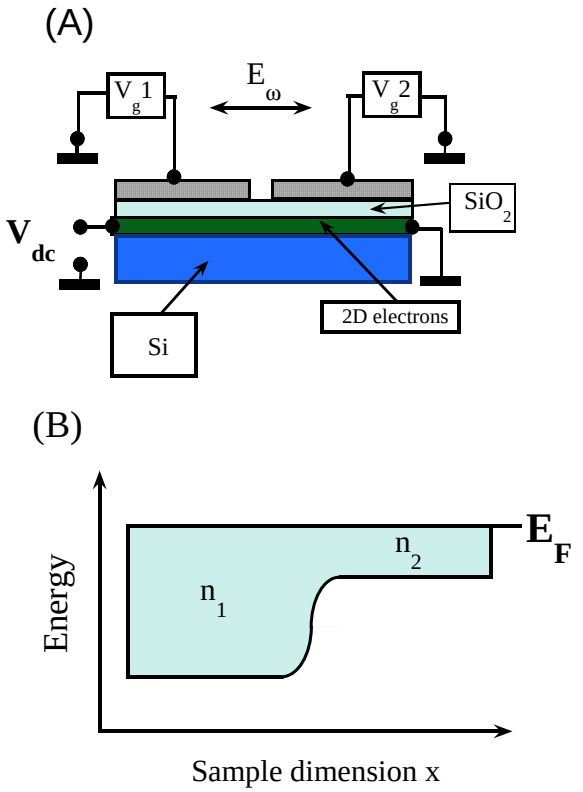

Figure 22: (a) Cross-section of the sample. Two different 2D metals are formed under the two separate gates with voltages V_g1 and V_g2 applied as shown. The rectified dc voltage V_{dc} is measured between the right and left ends of the structure. The microwave voltage is applied directly to the gates and is localized near the slit between them (see Fig. 21); (b) the Fermi level and bottom of the conduction band are shown as a function of position x along the sample. Energies below the Fermi level correspond to occupied electron states of the two 2D metals with different electron densities n_1 and n_2. The spatial variation of the electron density is described by Eq.(84).

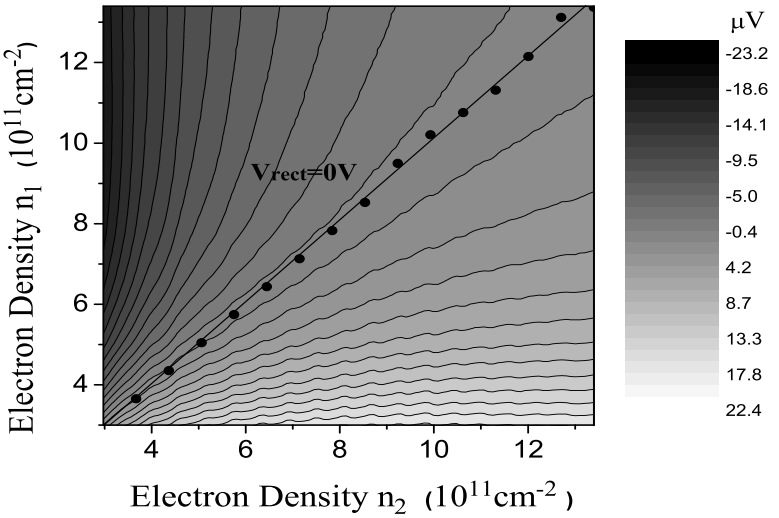

Figure 23: "Topological map" of the rectified voltage as a function of the electron densities n_1 and n_2. The rectified voltage is indicated by the shading, ranging from dark to light as the voltage varies from negative to positive. Measurements were taken at temperature 4.2 K, frequency 20.2 GHz, and microwave power input of 26 dB (specified relative to 1 mW for 0 dB). The rectification is an odd function of the difference between the two densities n_1 and n_2 (see Eq.(86)). The black dots denote the values of n_1 and n_2 for which the rectified signal changes polarity (goes through zero).

samples, the exact solution differs from Eq.(84) by less than 3%. The six different pairs of 2D electron systems studied displayed similar behavior.

Measurements were taken at frequencies from 0.7 GHz to 20 GHz in a vacuum chamber of a He-3 cryostat. The microwave radiation was guided by a semi-rigid coaxial line terminated by a loop. Two wires, anchored to a temperature controlled cold finger, were inductively coupled to the loop without touching it. The wires were connected directly to the two adjacent gates. The sample, with a calibrated RuO_2 thermometer attached, was thermally connected to the same cold finger. The temperature of the electrons was monitored using the amplitude of Shubnikov de Haas (SdH) oscillations. Without microwave power input, the electron temperature followed the temperature of the cold finger down to the lowest temperature $T = 0.27$ K. The sample was thus well isolated from heat input deriving from the coaxial line and the RF filtered DC electrical leads.

Rather than the resistance, the dominant contribution to the output impedance Z_{out} of the circuit at the end of the microwave line was provided by the (substantial) capacitive coupling between the two closely placed wires. Estimates indicated that variations of the resistivity of the 2D electrons with temperature and gate voltage have a negligibly small effect on Z_{out}. We therefore neglected the consequent small changes of output voltage V_{ac}. In particular, we neglected the effect of overheating the 2D electrons by the microwaves and consider the amplitude of the microwave voltage V_{ac} applied to the gates to be proportional to the square root of the calibrated microwave power P applied at the input of the coaxial line:

$$V_{ac} = G \cdot P^{1/2}, \tag{85}$$

where G is a temperature independent coefficient.

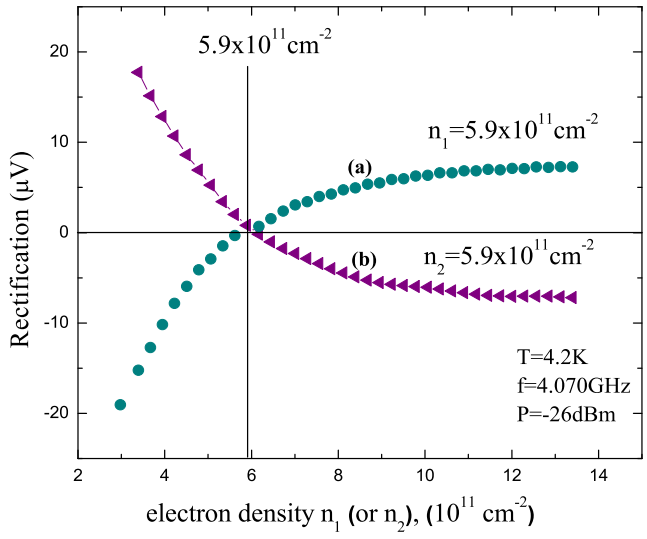

Figure 24: The open circles denote the rectified signal as a function of the electron density n_2 with electron density n_1 kept constant at $5.9 \times 10^{11} cm^{-2}$. The triangles show the rectified signal versus the electron density n_1 with the density n_2 fixed at the same value $5.9 \times 10^{11} cm^{-2}$. Measurements were taken at temperature 4.2 K, frequency 4 GHz, and microwave power 26 dB (specified relative to 1 mW for 0 dB). Note that if n_1 and n_2 are interchanged the rectification changes sign and satisfies relation (86).

The microwave-induced DC voltage was measured between two electrical contacts placed on opposite sides of the sample at a distance $L = 240\mu$m from the gap between the two electron systems (see Fig. 22(A)). To avoid thermoelectric effects related to the electrical contacts, the distance L must be considerably longer the thermal relaxation length L_T, which is estimated to be $L_T \sim$100 μm in Si-MOSFETs at temperatures of $\sim$ 1 K [62, 63, 72] (see Fig. 21). In this work we present data obtained at temperatures above 2 K, where the contact thermoelectricity is negligibly small.

The same results for the rectification were obtained using continuous microwave radiation and by modulating the microwave amplitude at frequency typically 10Hz and using standard phase sensitive techniques. All the data reported in this work were obtained by the second method, as it provided better detection of signals below $1\mu V$.

5.4 Experimental Results

5.5 Dependence of the rectification on electron density

Figure 23 shows the dependence of the rectified signal on the electron densities of the two adjacent 2D metals. The axes denote the electron densities n_1 and n_2, and the shading reflects the amplitude of the rectified signal, with dark (light) shading denoting negative (positive) values. Each horizontal scan was obtained for a fixed density n_1 (the electrons in the left-hand region of Fig. 22(A)), while the electron density n_2 in the adjacent (right-hand) region is varied. Shown by the black dots in Fig. 23, the DC voltage changes sign when the electron densities of the two 2D metals are nearly the same.

We note that similar results were obtained in our previous experiments [65], where microwave radiation was applied by a very different method using two parallel wires placed far from the samples. This indicates that the results are robust and do not

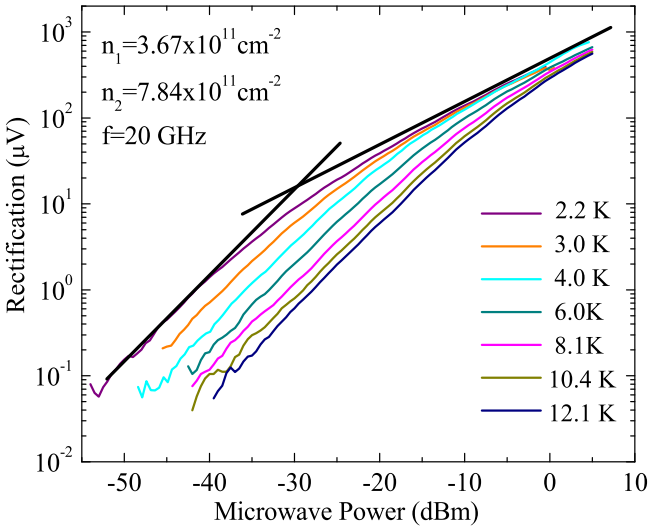

Figure 25: Rectified voltage as a function of microwave power on a log-log scale. The units of power are specified relative to 0 dB for 1 mW. Curves are shown for seven different temperatures ranging from 2.2 K (top curve) to 12.1 K (bottom curve). The straight lines represent linear P and square root $P^{1/2}$ dependence of the rectification on microwave power P. The electron densities are $- = 3.67 \times 10^{11}$ cm^{-2}, $n_2 = 7.84 \times 10^{11}$cm^{-2}. The microwave frequency is 20 GHz.

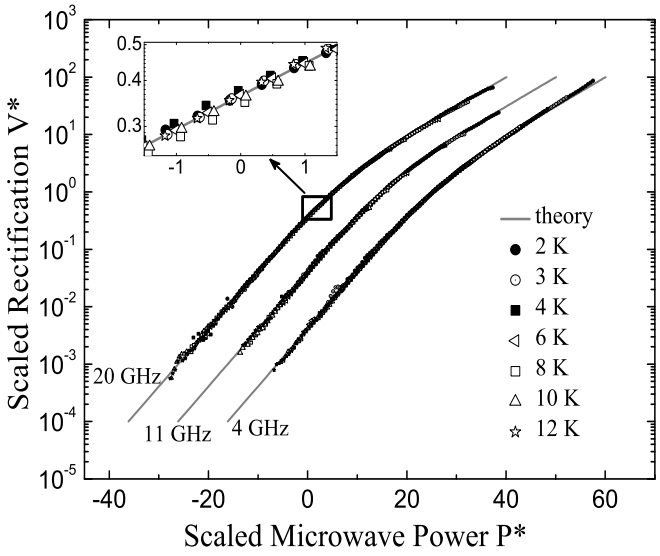

Figure 26: Normalized rectified voltage V^*_{dc} versus normalized microwave power P^* for frequencies 20 GHz (the data of Fig. 25), 11 GHz and 4 GHz at different temperatures. The data for frequencies 11 GHz and 4 GHz are shifted horizontally by 10 dB and 20 dB respectively with respect to the curve at 20 GHz for clarity. The solid lines are theoretical curves given by Eq.(81) and Eq.(82) (also shifted by 10 dB and 20 dB). The inset is a magnification of a portion of the top curve to indicate the quality of the scaling and/or typical deviations from the theory. A scaled curve is obtained at each frequency for all temperatures, and an appropriate horizontal shift brings the curves into alignment onto a single universal curve for all frequencies shown.

depend on details of the distribution of electromagnetic fields in the vicinity of the sample and that the dissimilarity between the two metals rather than the microwave field distribution is responsible for the effects observed. Moreover, the absence of rectification when $n_1 = n_2$ is strong experimental indication that bulk rectification inside the 2D metals, associated with microwave modulation of the electron density and/or mobility, is a minor contribution to the observed signal. This is discussed further below.

Figure 24 provides a clear demonstration that the rectified signal is an odd function of the difference $\Delta n = (n_2 - n_1)$ between the electron densities of the two systems. Here curve (a) shows the rectification when the electron density n_1 is fixed at $5.9 \times 10^{11} cm^{-2}$ while the electron density n_2 is varied; curve (b) is for fixed density $n_2 = 5.9 \times 10^{11} cm^{-2}$ and variable density n_1. Almost perfect antisymmetry is found with respect to the horizontal axis, showing that the rectification is an odd function of the difference between the two electron densities:

$$V_{dc}(n_1 - n_2) = -V_{dc}(n_2 - n_1), \tag{86}$$

5.6 Dependence of the rectification on microwave power at different temperatures

Figure 25 shows the rectified voltage as a function of microwave power on a log-log scale for seven different temperatures ranging from 2.2 K to 12 K at microwave frequency 20 GHz [73]. At all temperatures, the rectified signal for low power input is proportional to the microwave power (the square of the microwave electric field), $V_{dc} \propto P \propto E_\omega^2$. We will refer to this as the weak, or perturbative, nonlinear regime. Strongly nonlinear behavior is observed at higher levels of microwave excitation; here the rectified signal is

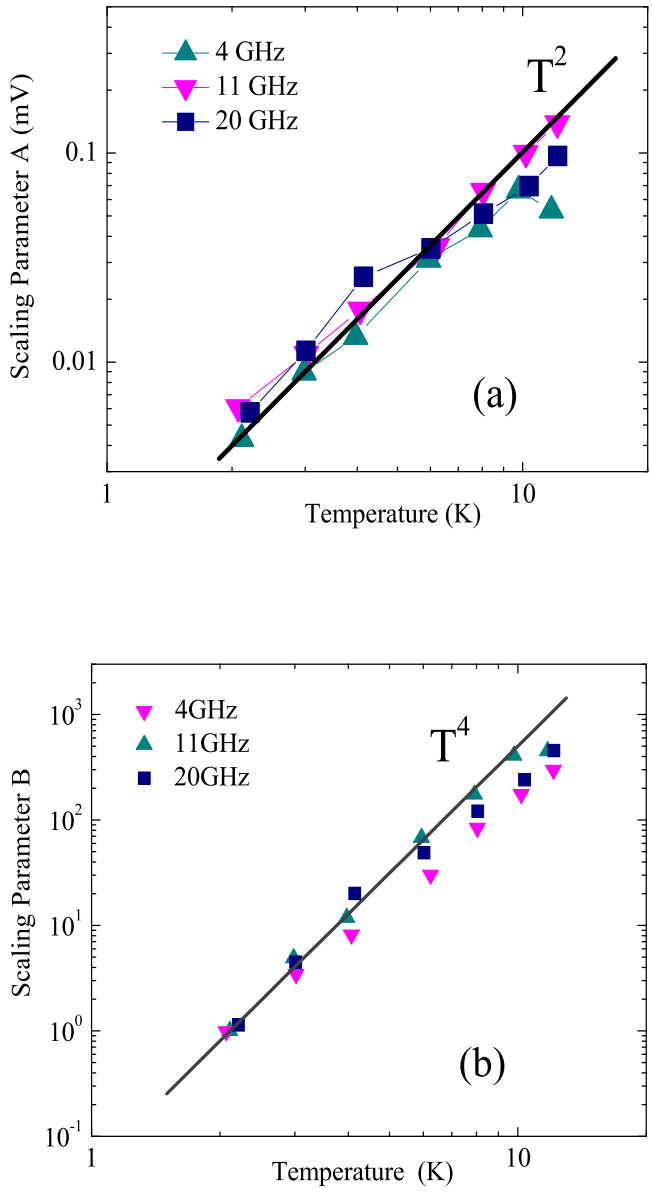

Figure 27: (A) Dependence of scaling parameter A on temperature at different frequencies, as labeled. The units of A are chosen to conform to the theoretical prediction of Eq.(70). The solid straight line is theoretical dependence corresponding to Eq.(71); (B) Dependence of scaling parameter B on temperature at different frequencies as labeled. Solid straight line is theoretical dependence corresponding to Eq.(78) with the parameter $R \sim T_L^6$.

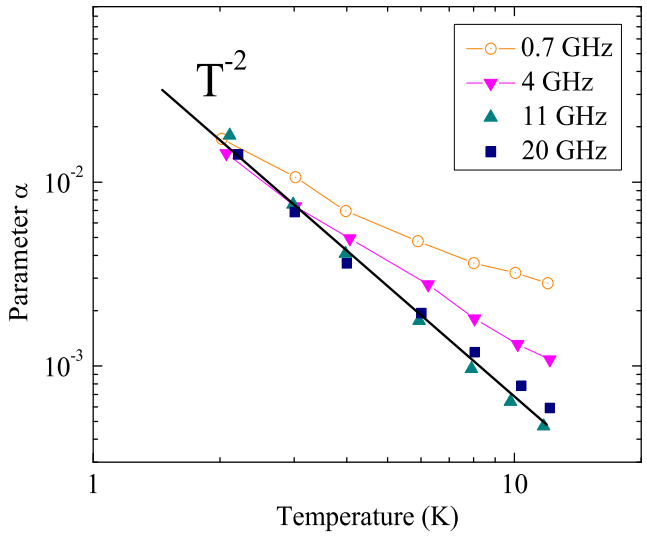

Figure 28: Temperature dependence of the proportionality constant, α, in the low microwave power regime where $V = \alpha \times P$. For 11 GHz and 20 GHz, $\alpha \sim T^{-2}$; the straight line corresponds to the theoretical prediction (Eq.(70) and Eq.(77)) at high frequencies. The electron densities are $n_1 = 3.67 \times 10^{11}$ cm^{-2} and $n_2 = 7.84 \times 10^{11}$ cm^{-2}.

proportional to the square root of the power, $V_{dc} \propto P^{1/2} \propto E_\omega$. The two straight lines drawn in Fig. 25 represent the two limits, namely, the perturbative ($V_{dc} \sim P$) and the strongly nonlinear ($V_{dc} \sim P^{1/2}$) regimes. The crossover between the two regimes depends on temperature, with the crossover occurring at higher microwave power as the temperature is increased.

By applying appropriate multiplicative scale factors (corresponding to translations on a log-log plot) to each of the curves of Fig. 25, one can collapse all the data for rectified voltage versus power at frequency 20 GHz onto the single universal curve:

$$V^*_{dc} = F(P^*), \tag{87}$$

as shown in Fig. 26. Also shown in Fig. 26 are similarly scaled curves for frequencies 11 GHz and 4 GHz.

The scaled values of the rectified voltage $V^*_{dc} = V/A(T)$ and power $P^* = P/B(T)$, require the two scaling parameters $A(T)$ and $B(T)$ shown in Fig. 27 as a function of temperature for different frequencies. For temperatures below 6 K the parameters $A(T) \propto T^2$ and $B(T) \propto T^4$, with deviations toward a weaker dependence at higher temperatures. There is no clear dependence on frequency. At a lower frequency (0.7GHz) the scaling breaks down for high power input, with substantial deviations from $V_{dc} \propto P^{1/2}$ behavior (not shown).

In the low power regime the rectification is found to be proportional to microwave power at all frequencies. In this weakly nonlinear regime, the rectification can be written as:

$$V_{dc} = \alpha(T) \times P, \tag{88}$$

where $\alpha(T)$ depends on the temperature. Figure 28 shows the constant of proportionality α plotted as a function of temperature for different frequencies.

The scaling behavior indicates (see Fig. 26) that $V_{dc}^{*} = \gamma \cdot P^{*}$ in the weak nonlinear regime with a constant, temperature-independent γ. Since the scaling parameters A and B are given by $V_{dc}^{*} = V/A(T)$ and $P^{*} = P/B(T)$ it follows that the coefficient $\alpha = \gamma \cdot \frac{A(T)}{B(T)}$. The solid line shows the behavior expected from the theory in the scaling regime.

5.7 Discussion

In the preceding sections, we reported measurements of the rectification of microwave radiation at the boundary between two-dimensional electron systems separated by a narrow gap between independently controlled gates on a silicon surface. The rectified signal is large, it is odd with respect to the interchange of the gates and, within a broad range of temperatures and frequencies, all data for the rectified voltage versus microwave input power collapse onto a single universal curve using two scaling parameters.

The fact that interchanging the gates gives rise to a signal that is essentially the same in magnitude and of opposite sign indicates that bulk rectification of the incoming microwave signal is a small contribution. Contrary to expectations for bulk rectification, the observed signal changes sign, does not depend on the detailed geometry of the sample and gates, and does not depend on the size of the sample. Moreover, as shown in the section on theory, we estimate that bulk rectification would contribute a signal that is considerably smaller than the mechanism we propose. It should be noted further that our observations cannot be attributed to rectification by non-ohmic contacts, as this would yield a signal that depends on the microwave field distribution along the sample and, therefore, should not be simply antisymmetric when the gates are interchanged.

The near-perfect antisymmetry of the rectification on interchanging gates, the fact that

the microwave power is strongly localized near the boundary between the 2D metals and the excellent agreement with theory, all provide strong evidence that the observed rectification is an inherent property of the two adjacent 2D electron systems of different densities. In particular, we attribute the observed rectification to a thermoelectric response due to strong local overheating of the electron gas that produces a large thermal gradient at the gap between the gates, where the electron density changes abruptly. We now proceed to present a detailed comparison between this theory and the experimental results.

As shown in Fig. 26, data for the rectified voltage versus input power can be collapsed over a broad range of temperature and microwave power onto a single universal curve using two scaling parameters. Plots of Eq.(81) and Eq.(82), are shown by the solid line. Excellent agreement is obtained between theory and experiment in a broad range of temperatures and the microwave power.

The scaling coefficients $A(T)$ and $B(T)$ used to obtain the data collapse vary with temperature, as shown in Fig. 27. The temperature dependence of parameter $A(T)$ denoted by the solid line in Fig. 27 (A), is proportional to T^2, in agreement with Eq.(71). At $T = 3$ K the scaling parameter $A(3K) = 10\mu$V, in good agreement with the theoretical estimate obtained using the Fermi energy E_F and the parameter β =0.2 for $n_1 = 3.67 \times 10^{11} cm^{-2}$ for Si-MOSFETs[74]. At higher temperatures ($\sim$ 10K) the experimental values of A tend to fall below the theory because of a noticeable part of the heat emits in the region $\pm l_{ac}$. We also note that for electron density $n_1 = 3.67 \times 10^{11} cm^{-2}$ the Fermi energy in Si-MOSFETS is about 20 K so that at $T \sim 10K$ the electron system is not strongly degenerate and finite temperature corrections to the thermoelectric coefficient Q (see Eq.(69)) and the Wiedemann-Franz ratio have to be taken into account.

Surprisingly, the theory gives much better scaling than one would expect from the

accuracy of both the thermopower coefficient Q and the Wiedemann-Franz relation. This may reflect the fact that acoustic phonon scattering is quasi-elastic and hot electrons remain in the "energy quasi-ballistic" regime [70]. A careful analysis of the electron kinetics is required to verify this.

The scaling parameter $B(T)$ is shown in Fig. 27(B). The parameter B displays similar behavior as a function of temperature for all measured frequencies above 4 GHz. The temperature dependence is due to the strong dependence of the power losses $F(T) = R_1(T^6 - T_L^6)$ on the lattice temperature. The solid line shows the theoretical expectation using an approximation of the power losses by Eq.(73) derived from recent theory [62] and experiment [63]. At higher temperatures discrepancies between theory and experiment are seen, which are, most likely, associated with deviations from scaling at low frequencies, for reasons discussed below.

Fig.28 shows the temperature dependence of the parameter α, the constant of proportionality that relates the rectified voltage V_{dc} to the microwave power P in the weakly nonlinear regime (see Eq.(88)). In accordance with the theory (see Eq.(80)), the coefficient α is proportional to the ratio between the scaling parameter A to the parameter B: $\alpha(T) \propto A(T)/B(T) \propto 1/T^2$; the theoretically expected behavior is shown in the figure by the solid straight line. Good agreement with theory is obtained at high microwave frequencies (>10 GHz), where the microwave radiation is well localized near the boundary between the two 2D metals. However, progressively stronger deviations from the theory develop as the frequency is decreased. These deviations correlate with deviations from the scaling regime observed at frequencies below 4 GHz.

In particular at frequency 0.7 GHz the power dependence of rectification at high power does not follow the $P^{1/2}$ rule and the universality governed by Eq.(81) and Eq.(82) is not observed. We suggest that the observed departures from theoretical expectations are due to the fact that the experimental results are outside the range of validity

of the theory in its present form. Analytical and numerical estimates indicate that at low frequency (1 GHz and below) the microwave field is barely localized near the boundary between the two 2D metals. The corresponding size of the hot strip at frequency $1GHz$ is $l_{ac} \sim 80\ \mu$ is considerably broader than the temperature relaxation length L_T, especially in the high temperature domain (several microns at T >6 K). For these conditions, one of the central approximations of the theory ($l_{ac} \ll L_T$) is no longer valid.

5.8 Summary

We have measured the rectification of microwave radiation (0.7-20 GHz) at the boundary between two-dimensional electron systems with different electron densities. For frequencies above 4 GHz and over a broad range of temperatures and microwave power, the rectified voltage V_{dc} obeys two-parameter scaling: the power dependence obtained at different temperatures and frequencies collapse onto a single universal curve $V_{dc}^* = F(P^*)$. Over the range investigated in these experiments, the scaling exhibits two different power regimes. For small power the voltage is a linear function of power, $V_{dc}^* \sim P^*$, while at higher power the rectification is proportional to $(P^*)^{1/2}$. A theory is proposed that attributes the rectification to the thermoelectric response caused by strong local overheating of the 2D electrons by the microwave radiation at the boundary between two dissimilar 2D metals. Excellent agreement is obtained between theory and experiment.

6 Conclusions

The research presented describes three experiments which focus on the non-linear properties of two dimensional electron systems. In the first experiment the non-linear zero-differential resistance state (ZDRS) that occurs for a GaAs quantum well in the presence of a magnetic field and an electric dc bias was studied. It was found that when the magnetic field is strong and is applied perpendicular to the electron plane, this ZDRS is suppressed and disappears gradually as the magnetic field is tilted away from the perpendicular at a fixed filling factor ν (at a fixed perpendicular magnetic field component). The experimental results were explained with the use of a theoretical model that considers spectral diffusion of the electrons, as well as the effect of the Zeeman splitting of Landau levels enhanced by the total magnetic field.

In the second experiment measurements on three GaAs quantum wells were performed. Measurements of the electric dc field applied while maintaining a constant temperature, versus varying the temperature while keeping the electric field constant, are presented. It is shown that the electric field applied produces a non-equilibrium electron distribution, which cannot be described by an elevated temperature. The electron distribution changes significantly the conductivity of highly mobile two dimensional electron systems in the presence of a magnetic field, and it forces them into a state with a zero differential resistance. Moreover, the results demonstrate that in general, the effective overheating in systems with a discrete spectrum is much stronger than the one in systems with continuous and homogeneous distribution of the energy levels at the same input power.

In the third experiment we studied another non-linear effect on a high-mobility Si-MOSFET. We measured the rectification of microwave radiation at the boundary between two-dimensional electron systems with different electron densities. It was

found that over a broad range of frequencies, temperatures and microwave powers, the rectified voltage V_{dc} obeys two-parameter scaling: the power dependence obtained at different temperatures and frequencies collapse onto a single universal curve $V_{dc}^{*} = F(P^{*})$. Over the range investigated in these experiments, the scaling exhibits two different power regimes. For small power the voltage is a linear function of power, $V_{dc}^{*} \sim P^{*}$, while at higher power the rectification is proportional to $(P^{*})^{1/2}$. We obtained excellent agreement with a theory that attributes the rectification to the thermoelectric response caused by strong local overheating of the 2D electrons by the microwave radiation at the boundary between two dissimilar two-dimensional metals.

References

[1] N. Romero, S. McHugh, M. P. Sarachik, S. A. Vitkalov, and A. A. Bykov, Phys. Rev. B **78**, 153311 (2008).

[2] M. G. Vavilov and I. L. Aleiner Phys. Rev. B **69**, 035303 (2004).

[3] N. Romero, A. A. Bykov, Sergey Vitkalov, and A. I. Toropov, Phys. Rev. B **78**, 085306 (2008).

[4] N. Romero, I. Hoxha, Y. Jin, S. A. Vitkalov, M. P. Sarachik, Ivan A. Larkin, and T. M. Klapwijk, Phys. Rev. B **77**, 035415 (2008).

[5] Y. Imry, *Introduction to Mesoscopic Physics*, Oxford University Press, Cambridge 1997; 2nd edition 2002.

[6] S. Datta, *Electronic Transport in Mesoscopic Systems*,Cambridge University Press, Cambridge, 1997.

[7] E. O'Reilly *Quantum Theory of Solids*, Taylor and Francis, 2002.

[8] E. Cage, R. F. Dziuba and B. F. Field (1985), IEEE Trans. Instrum. Meas. **IM-34**, 301.

[9] N. W. Ashcroft, N. D. Mermin, *Solid State Physics*, Holt, Rinehart and Winston, 1976.

[10] J. M. Ziman, *Principles of the theory of solids*, Cambridge at the university press, 1972.

[11] M. A. Zudov, R. R. Du, J. A. Simmons, and J. L. Reno, Phys. Rev. B **64**, 201311(R) (2001).

[12] P. D. Ye, L. W. Engel, D. C. Tsui, J. A. Simmons, J. R. Wendt, G. A. Vawter, and J. L. Reno, Appl. Phys. Lett. **79**, 2193 (2001).

[13] R. G. Mani, J. H. Smet, K. von Klitzing, V. Narayanamurti, W. B. Johnson, V. Umansky, Nature (London) 420, 646 (2002).

[14] M. A. Zudov, R. R. Du, L. N. Pfeiffer, and K.W. West, Phys. Rev. Lett. **90**, 046807 (2003).

[15] S. I. Dorozhkin, JETP Lett. **77**, 577 (2003).

[16] R. L. Willett, L. N. Pfeiffer, and K.W. West, Phys. Rev. Lett. **93**, 026804 (2004).

[17] A.V. Andreev, I. L. Aleiner, and A. J. Millis, Phys. Rev.Lett. **91**, 056803 (2003).

[18] A. C. Durst, S. Sachdev, N. Read, and S. M. Girvin, Phys. Rev. Lett. **91**, 086803 (2003).

[19] X. L. Lei and S. Y. Liu, Phys. Rev. B **72**, 075345 (2005).

[20] P.W. Anderson and W. F. Brinkman, arXiv:cond-mat/ 0302129.

[21] J. Shi and X. C. Xie, Phys. Rev. Lett. **91**, 086801 (2003).

[22] I. A. Dmitriev, M. G. Vavilov, I. L. Aleiner, A.D. Mirlin, and D. G. Polyakov, Phys. Rev. B **71**, 115316 (2005).

[23] C. L. Yang, J. Zhang, R. R. Du, J. A. Simmons, and J. L. Reno, Phys. Rev. Lett. **89**, 076801 (2002).

[24] A. A. Bykov, J. Zhang, S. Vitkalov, A. K. Kalagin and A. K. Bakarov, Phys. Rev. B **72**, 245307 (2005).

[25] J. Zhang, S. Vitkalov, A. A. Bykov, A. K. Kalagin, and A. K. Bakarov, Phys. Rev. B **75**, 081305(R) (2007).

[26] W. Zhang, H.-S. Chiang, M. A. Zudov, L. N. Pfeiffer, and K.W. West, Phys. Rev. B **75**, 041304(R) (2007).

[27] A. A. Bykov, J. Q. Zhang, S. Vitkalov, A. K. Kalagin and A. K. Barakov, Phys. Lett. **99**,116801 (2007).

[28] W. Zhang, M. A. Zudov, L. N. Pfeiffer, and K. W. West,Phys. Rev. Lett. **100**, 036805 (2008).

[29] M. G. Vavilov, I. L Aleiner, and L. I. Glazman, Phys. Rev. B **76**, 115331 (2007).

[30] Jing-qiao Zhang, Ph.D. Thesis, The City University of New York (2009).

[31] C. L. Yang, R. R. Du, L. N. Pfeiffer, and K. W. West, Phys. Rev. B **74**, 045315 (2006).

[32] R. G. Mani, Phys. Rev. B 72, 075327 (2005).

[33] S. A. Vitkalov , H. Zheng, K. M. Mertes, M. P.Sarachik, and T. M. Klapwijk, Phys. Rev. Lett. **85**, 2164, (2000).

[34] M. E. Raikh and T. V. Shahbazyan, Phys. Rev. B **47**, 1522 - 1531 (1993).

[35] T. Ando, Y. Uemura, J. Phys. Soc. Japan, **36**, 959, (1974).

[36] M. M. Fogler, A. Yu. Dobin, V. I. Perel, and B. I. Shklovskii Phys. Rev. B **56**, 6823 - 6838 (1997).

[37] Y. W. Tan, J. Zhu, H. L. Stormer, L. N. Pfeiffer, K. W. Baldwin, and K. W. West Phys. Rev. B **73**, 045334 (2006).

[38] I. A. Dmitriev, A. D. Mirlin, and D. G. Polyakov, Phys. Rev. B **75**, 245320 (2007).

[39] I. B. Levinson Soviet Physics-Solid State **6**, 1665 (1965).

[40] Peter J. Price J. Appl. Phys. **53**, 6863 (1982).

[41] L. D. Landau, E. M. Lifshitz "Quantum Mechanics: Nonrelativistic Theory", Pergamon Press (1997).

[42] D. Shoenberg "Magnetic oscillations in metals", Cambridge University Press (1984).

[43] T. Ando, A.B. Fowler and F. Stern Review of Modern Physics, **54**,437 (1982).

[44] In strong magnetic fields the longitudinal resistance r_{xx} is proportional to longitudinal conductivity σ [22]. In this treatment we consider these two terms to be similar.

[45] S. Studenikin Phys. Rev. B **71**, 245313, (2005).

[46] A. A. Bykov, A. K. Bakarov, D. R. Islamov, A. I. Toropov, JETP Letters **84**, 391 (2006).

[47] A. Auerbach, I. Finkler, B. I. Halperin, and A. Yacoby, Phys. Rev. Lett. **94**, 196801 (2005).

[48] J. Alicea, L. Balents, M.P.A. Fisher, A. Paramekanti, L. Radzihovsky, Phys. Rev. B **71**, 235322 (2005).

[49] M.G. Vavilov, I.L Aleiner, and L.I. Glazman, cond-mat/0611130.

[50] L. DiCarlo, C.M. Marcus and J. S. Harris, Jr., Phys Rev. Lett. **91**, 246804 (2005).

[51] J.Wei, M. Shimogawa, Z. Wang, I. Radu, R. Dormaier, and D. H. Cobden, Phys. Rev. Lett. **95**, 256601 (2005).

[52] R. Leturcq, D. Sanchez, G. Gotz, T. Ihn, K. Ensslin, D. C. Driscoll, and A. C. Gossard, Phys. Rev. Lett. **96**, 126801 (2006).

[53] D. M. Zumbhl, C. M. Marcus, M. P. Hanson and A. C. Gossard, Phys. Rev. Lett. **96**, 206802 (2006).

[54] A. Lofgren, C. A. Marlow, I. Shorubalko, R. P. Taylor, P. Omling, L. Samuelson, and H. Linke, Phys. Rev. Lett. **92**, 046803 (2004).

[55] J.Q. Zhang, S. Vitkalov, Z. D. Kvon, J. C. Portal, and A. Wieck, Phys. Rev. Lett. **97**, 226807 (2006).

[56] P. W. Brouwer, Phys. Rev. B **63**,121303(R) (2001).

[57] M. G. Vavilov, V. Ambegaokar and I. L. Aleiner Phys. Rev. B **63**,195313 (2001).

[58] D. Sanchez and M. Buttiker, Phys. Rev. Lett. **93**,106802 (2004).

[59] B. Spivak and A. Zyuzin, Phys. Rev. Lett **93**, 226801 (2004).

[60] M. L. Polianski and M. Buttiker Phys. Rev. Lett. **96**, 156804 (2006).

[61] A. V. Andreev and L. I. Glazman cond-mat/060861 (2006).

[62] A. Sergeev, M. Yu. Reizer, V. Mitin, Phys. Rev. Lett. **94**, 136602, (2005).

[63] R. Fletcher, V. M. Pudalov, Y. Feng, M. Tsaousidou, and P. N. Butcher, Phys. Rev. B **56**, 12422 (1997).

[64] V C Karavolas, P N Butcher J. Phys Condensed Matter, **2**,3947 (1990).

[65] I. Hoxha, S. A. Vitkalov, N. A. Zimbovskaya, M. P. Sarachik and T. M. Klapwijk, cond-mat/0110331.

[66] I. A. Larkin, S. A. Vitkalov and M.P. Sarachik, Brazilian Journal of Physics **x**, xxxxx, (2007).

[67] J. H. Davies, I. A.Larkin, E. V. Sukhorukov, J. Appl. Phys. **77**, 4504 (1995).

[68] V. I. Falko Sov. Phys. Solid State **31**, 561 (1989).

[69] N. A. Zimbovskaya Phys. Rev. **B**, 113404 (2003).

[70] Yu. Dubrovskii, I. A. Larkin and S. Morosov, Superlatt. Microstruct. 8, 233, (1991).

[71] J. H. Davies, I. A.Larkin, Phys. Rev. B **49**, 4800 (1994).

[72] O. Prus, M. Reznikov, U. Sivan, and V. Pudalov Phys. Rev. Lett. **88**, 016801 (2002).

[73] For temperatures T <4K the data were obtained in a small magnetic field of 0.4 T to suppress superconductivity of the aluminum gates and avoid the change (about 20%- 30%) of the microwave field E_ω near the sample due to a superconducting transition [65].

[74] V. K. Karavolas, M. J. Smith, T. M. Fromhold, P. N. Butcher, B. G. Mulimani, B. L. Gallagher and J. P. Oxley, J. Phys.: Condens. Matter **2**, 10401 (1990).